

**POLITECNICO DI TORINO**

**Master's Degree in Mechanical Engineering**



**Master's Degree Thesis**

**Extraction and Automatic Selection of Modal  
Parameters**

**Supervisor**

**Prof. Alessandro FASANA**

**Candidate**

**Yang CAO**

**December 2022**



# Table of Contents

<b>Chapter 1 - Definition of a multi-degrees-of-freedom system</b>	<b>1</b>
<b>Chapter 2 - Comparison of the two different integration procedures</b>	<b>5</b>
<b>Chapter 3 - Comparison of modal parameters extraction methods</b>	<b>16</b>

# Chapter 1 - Definition of a multi-degrees-of-freedom system

To implement the modal parameter extraction that will be discussed in the thesis, we need to define the system of interest, i.e., the research object, first. It is necessary for two reasons:

- a defined system, whose modal parameters are already available to the readers, can be a good benchmark to the various methods of modal parameter extraction;
- the very procedure of defining a system can help the readers to understand the physical meanings of the modal parameters.

Therefore, in this chapter, the full description of defining a typical multiple-degrees-of-freedom (MDOF) mechanical system will present. It will be implemented through examples together with corresponding MATLAB codes.

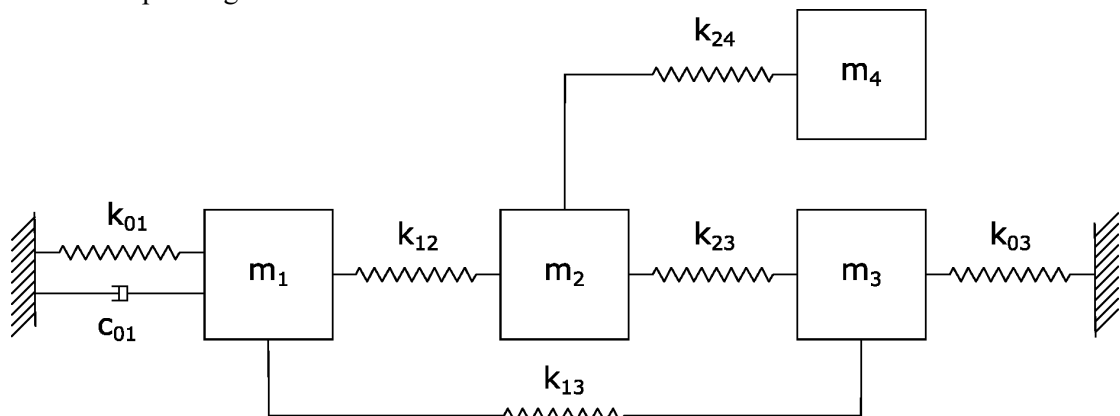


Fig1.1 A typical MDOF mechanical system with masses, springs, and dampers.

**Fig.1.1** depicts a typical 4-degrees-of-freedom (DOFs) mechanical system consisting of masses, springs, and dampers. To define such a system, two critical constants must be defined first. They are:

- the number of the masses, i.e., number of DOFs,  $n$ ;
- the number of the springs and dampers,  $n_k$ .

Here, the number of springs and of dampers share a same  $n_k$  because we consider they are always equal. In case they are physically not, for example as shown in Fig.1.1 where only a spring but no damper is present between mass 1 and 2, the corresponding damping factor is specified as zero so that the number of dampers does not decrease. The MATLAB codes corresponding to the example presented in Fig.1.1 can be seen as line-3 and -4 in listing 1.1.



After defining the numbers, the mass (**M**), stiffness (**K**), and damping (**C**) matrix can be given. Still, we can take the 4-DOF system depicted in Fig.1.1 as an example. The mass matrix is hence [4]:

$$\mathbf{M} = \begin{bmatrix} m_1 & 0 & 0 & 0 \\ 0 & m_2 & 0 & 0 \\ 0 & 0 & m_3 & 0 \\ 0 & 0 & 0 & m_4 \end{bmatrix}$$

Where  $m_1$ ,  $m_2$ ,  $m_3$ , and  $m_4$  are respectively the values of the four masses. See the MATLAB codes in line-7 to -11 of listing 1.1.

The definition of the stiffness and damping matrices is slightly trickier, as they are usually non-diagonal. As shown from line-14 to -19, the first step to define **K** and **C** is to specify their components  $k_{pq}$  and  $c_{pq}$  one by one according to the following rules:

- 1)  $k_{pq}$  refers to a spring connecting DOF-p and -q, the same to the  $c_{pq}$ ;
- 2) subscript  $p = 0$  indicates fixed supporting;
- 3) as mentioned above,  $k_{pq}$  and  $c_{pq}$  are equal to 0 if they are not presented.

Therefore, the subscript  $pq$  in fact suggests the links between masses. Furthermore, to help the program to access the links, a  $n_k \times 2$  matrix, i.e., **Mappa**, should be given by simply listing all these subscripts. For instance, in case of a system in Fig.1.1, this matrix can be:

$$\mathbf{Mappa} = \begin{bmatrix} 0 & 1 \\ 0 & 3 \\ 1 & 2 \\ 1 & 3 \\ 2 & 3 \\ 2 & 4 \end{bmatrix}$$

whose rows indicates the corresponding subscripts,  $p$  and  $q$ , of  $k_{pq}$  and  $c_{pq}$ . See the codes' details in line-22 and -23 of listing 1.1.

Then we need to assembly all the  $k_{pq}$  and  $c_{pq}$  components in the complete stiffness and damping matrix. To do so, a local matrix, **local**, is defined first as

$$\mathbf{local} = \begin{bmatrix} 1 & -1 \\ -1 & 1 \end{bmatrix}$$

which acts as a basic unit for a spring or damper between two masses. It comes from a basic case where only two masses and their link, a spring or a damper, present. As shown in Fig.1.2a, such a simple case owns equation of motion as following [4]:

$$\begin{bmatrix} m_1 & 0 \\ 0 & m_2 \end{bmatrix} \begin{Bmatrix} \ddot{x}_1 \\ \ddot{x}_2 \end{Bmatrix} + \begin{bmatrix} 1 & -1 \\ -1 & 1 \end{bmatrix} c_{12} \begin{Bmatrix} \dot{x}_1 \\ \dot{x}_2 \end{Bmatrix} + \begin{bmatrix} 1 & -1 \\ -1 & 1 \end{bmatrix} k_{12} \begin{Bmatrix} x_1 \\ x_2 \end{Bmatrix} = \begin{Bmatrix} 0 \\ 0 \end{Bmatrix}$$

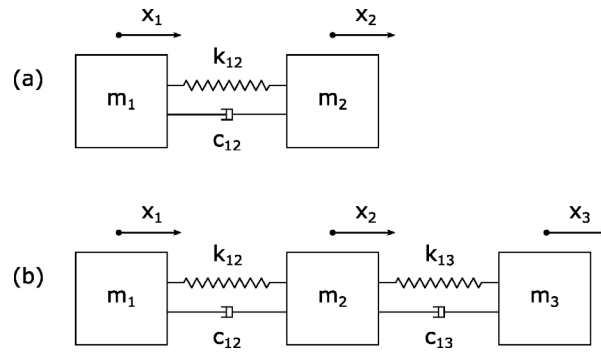
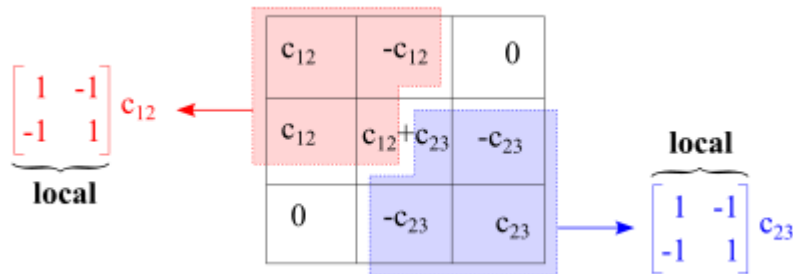


**Fig1.2** Schematic representation of a (a) 2- and (b) 3-DOF mechanical system with masses and springs and dampers in between.

As it can be seen, the matrix **local** occurs in both the second and third terms. When the number of masses increases, for instance for a 3-DOF system as shown in figure 1.2b, the global stiffness matrix can be assembled as [4]:

$$\begin{bmatrix} m_1 & 0 & 0 \\ 0 & m_2 & 0 \\ 0 & 0 & m_3 \end{bmatrix} \begin{Bmatrix} \ddot{x}_1 \\ \ddot{x}_2 \\ \ddot{x}_3 \end{Bmatrix} + \begin{bmatrix} c_{12} & -c_{12} & 0 \\ -c_{12} & c_{12} + c_{23} & -c_{23} \\ 0 & -c_{23} & c_{23} \end{bmatrix} \begin{Bmatrix} \dot{x}_1 \\ \dot{x}_2 \\ \dot{x}_3 \end{Bmatrix} + \begin{bmatrix} k_{12} & -k_{12} & 0 \\ -k_{12} & k_{12} + k_{23} & -k_{23} \\ 0 & -k_{23} & k_{23} \end{bmatrix} \begin{Bmatrix} x_1 \\ x_2 \\ x_3 \end{Bmatrix} = \begin{Bmatrix} 0 \\ 0 \\ 0 \end{Bmatrix}$$

Where the damping matrix can be decomposed as



Just like the stiffness matrix. It can be seen from this example how **local** matrix local performs as a basic unit for spring or damper between two masses.

Listing 1: MATLAB codes for system definition

```

1. % For a system depicted in fig. 1.1
2.
3. n = 4; % Number of dof
4. nk = 6; % Number of springs and dampers
5.
6. % Mass
7. m1 = 12;
8. m2 = 15;
9. m3 = 12;

```

```

10. m4 = 15;
11. m = diag([m1,m2,m3,m4]); % Mass matrix
12.
13. % Stiffness and damping
14. k01 = 100; c01 = 1*5;
15. k03 = 200; c03 = 2*5;
16. k12 = 300; c12 = 3*5;
17. k13 = 400; c13 = 0*5;
18. k23 = 500; c23 = 5*5;
19. k24 = 600; c24 = 6*5;
20.
21. % Links between masses
22. mappa = zeros(nk,2); % Preallocation
23. mappa = [0 1; 0 3; 1 2; 1 3; 2 3; 2 4]; % Links between masses
24.
25. local = [1 -1;-1 1]; % Local stiffness and damping matrix
26.
27. % Stiffness matrix
28. K = zeros(n+1); % Preallocation
29. for j = 1:nk
30.     coord = mappa(j,:)+1;
31.     eval(['k = k' num2str(mappa(j,1)) num2str(mappa(j,2)) ' ');
32. ])
33.     K(coord,coord) = K(coord,coord) + local*k;
34. end
35. K = K(2:n+1,2:n+1); % Border condition
36. clear k
37. k = K;
38. clear K;
39.
40. % Damping matrix
41. C0 = zeros(n+1);
42. for j = 1:nk
43.     coord = mappa(j,:)+1;
44.     eval(['c = c' num2str(mappa(j,1)) num2str(mappa(j,2)) ' ');
45. ])
46.     C0(coord,coord) = C0(coord,coord)+local*c;
47. end
47. c=C0(2:n+1,2:n+1); % Border condition

```

## Chapter 2 - Comparison of the two different integration procedures

In the previous chapter, we got the equations of motion of a typical MDOF mechanical system in the configuration space. Take Fig.1.2 (a) as an example, simplified Equation (1.1):

$$\mathbf{M}\{\ddot{x}\} + \mathbf{C}\{\dot{x}\} + \mathbf{K}\{x\} = \{f\} \quad (2.1)$$

where  $\{x\}$  is a vector in which the generalized coordinates are listed, and  $f$  is a time-dependent vector containing the forcing functions. This equation is from the point of view of mechanics. Now, let's look at it from another side, we know all  $\mathbf{M}$ ,  $\mathbf{C}$ , and  $\mathbf{K}$  of this system. So, we now analyze the same system in state space. Which is more intuitive observation and focus on input and output.

In this chapter, we compare two different methods to integrate the system, specifically, the discrete time linear system method and the Duncan method. Both of them transform the system characteristic equation from configuration space to state space after defining the mass, stiffness, and damping matrices.

From the configuration space to the state space, we introduce a set of auxiliary variables. The simplest one is to use  $\{\dot{x}\} = \{v\}$  which is a kinematic equation so that  $\{\ddot{x}\} = \{\dot{v}\}$  and therefore

$$\mathbf{M}\{\dot{v}\} + \mathbf{C}\{v\} + \mathbf{K}\{x\} = \{f\} \quad (2.2)$$

In the monic form is:

$$\{\dot{v}\} = -\mathbf{M}^{-1}\mathbf{C}\{v\} - \mathbf{M}^{-1}\mathbf{K}\{x\} + -\mathbf{M}^{-1}\{f\} \quad (2.3)$$

Then,

$$\begin{Bmatrix} \{\dot{v}\} \\ \{v\} \end{Bmatrix} = \begin{bmatrix} -\mathbf{M}^{-1}\mathbf{C} & -\mathbf{M}^{-1}\mathbf{K} \\ \mathbf{I} & \mathbf{0} \end{bmatrix} \begin{Bmatrix} \{v\} \\ \{x\} \end{Bmatrix} + \begin{bmatrix} \mathbf{M}^{-1} \\ \mathbf{0} \end{bmatrix} \{f\} \quad (2.4)$$

A state vector:

$$\{z\} = \begin{Bmatrix} \{\dot{x}\} \\ \{x\} \end{Bmatrix} = \begin{Bmatrix} \{v\} \\ \{x\} \end{Bmatrix} \quad (2.5)$$

Then, with reference to the state space, the equation of motion of a linear system can be transformed into a set of  $2n$  first-order linear differential equations, the state equations of the system:

$$\{\dot{z}\} = \mathbf{A}\{z\} + \mathbf{B}\{u\} \quad (2.6)$$

Therefore,

$$\mathbf{A} = \begin{bmatrix} -\mathbf{M}^{-1}\mathbf{C} & -\mathbf{M}^{-1}\mathbf{K} \\ \mathbf{I} & \mathbf{0} \end{bmatrix}; \mathbf{B} = \begin{bmatrix} \mathbf{M}^{-1} \\ \mathbf{0} \end{bmatrix} \quad (2.7)$$

Where matrix  $\mathbf{A}$  and  $\mathbf{B}$  indicate the dynamic and input gain matrix of the system.  $\{f\}$  is input vector usually defines as  $\{u\}$ .

Base on equation of motion of configuration space (2.1), for the Duncan method, the transformation is performed according to equations as follows:

Set,

$$\{y\} = \begin{Bmatrix} \{x\} \\ \{\dot{x}\} \end{Bmatrix}; \{\dot{y}\} = \begin{Bmatrix} \{\dot{x}\} \\ \{\ddot{x}\} \end{Bmatrix} \quad (2.8)$$

Substitute into the Equation (3.1):

$$(\mathbf{C} \ \mathbf{M})\{\dot{y}\} + (\mathbf{K} \ \mathbf{0})\{y\} = \{0\} \quad (2.9)$$

And,

$$\begin{bmatrix} \mathbf{C} & \mathbf{M} \\ \mathbf{M} & \mathbf{0} \end{bmatrix} \{\dot{y}\} + \begin{bmatrix} \mathbf{K} & \mathbf{0} \\ \mathbf{0} & -\mathbf{M} \end{bmatrix} \{y\} = \begin{Bmatrix} 0 \\ 0 \end{Bmatrix} \quad (2.10)$$

Then, a set of n second order differential equations can be transformed in a set of 2n first order differential equations:

$$\mathbf{A}\{\dot{y}\} + \mathbf{B}\{y\} = \{0\} \quad (2.11)$$

Therefor,

$$\mathbf{A} = \begin{bmatrix} \mathbf{C} & \mathbf{M} \\ \mathbf{M} & \mathbf{0} \end{bmatrix}; \mathbf{B} = \begin{bmatrix} \mathbf{K} & \mathbf{0} \\ \mathbf{0} & -\mathbf{M} \end{bmatrix} \quad (2.12)$$

The MATLAB implementations of the two different methods are respectively the **Integration.m** and **Duncan.m**. Their results respect to same working condition will be compared in the following part of this section.

Case 1. Only one random input

Considering the 4-degrees-of-freedom mechanical system that is already defined in Chapter 1, only one random force is applied onto the third mass. The MATLAB code of the forcing matrix of the discrete time linear system method is attached as following:

```
1. f=zeros(length(t),n);
2. f(:,3)=500*randn(length(t),1); % random input on mass 3
```

where  $t$  is the vector of time;  $n$  is the number of degrees of freedom. Then save the random input and apply it with the Duncan method. The elapsed time in MATLAB of the discrete time linear system method and the Duncan method is 0.242s and 0.105s (consider there are no noise on measurements). It can still be seen that the Duncan method is faster, even if the difference is small. And with such a random force, the two different methods give results as shown in Fig.2.1 and Fig.2.2.

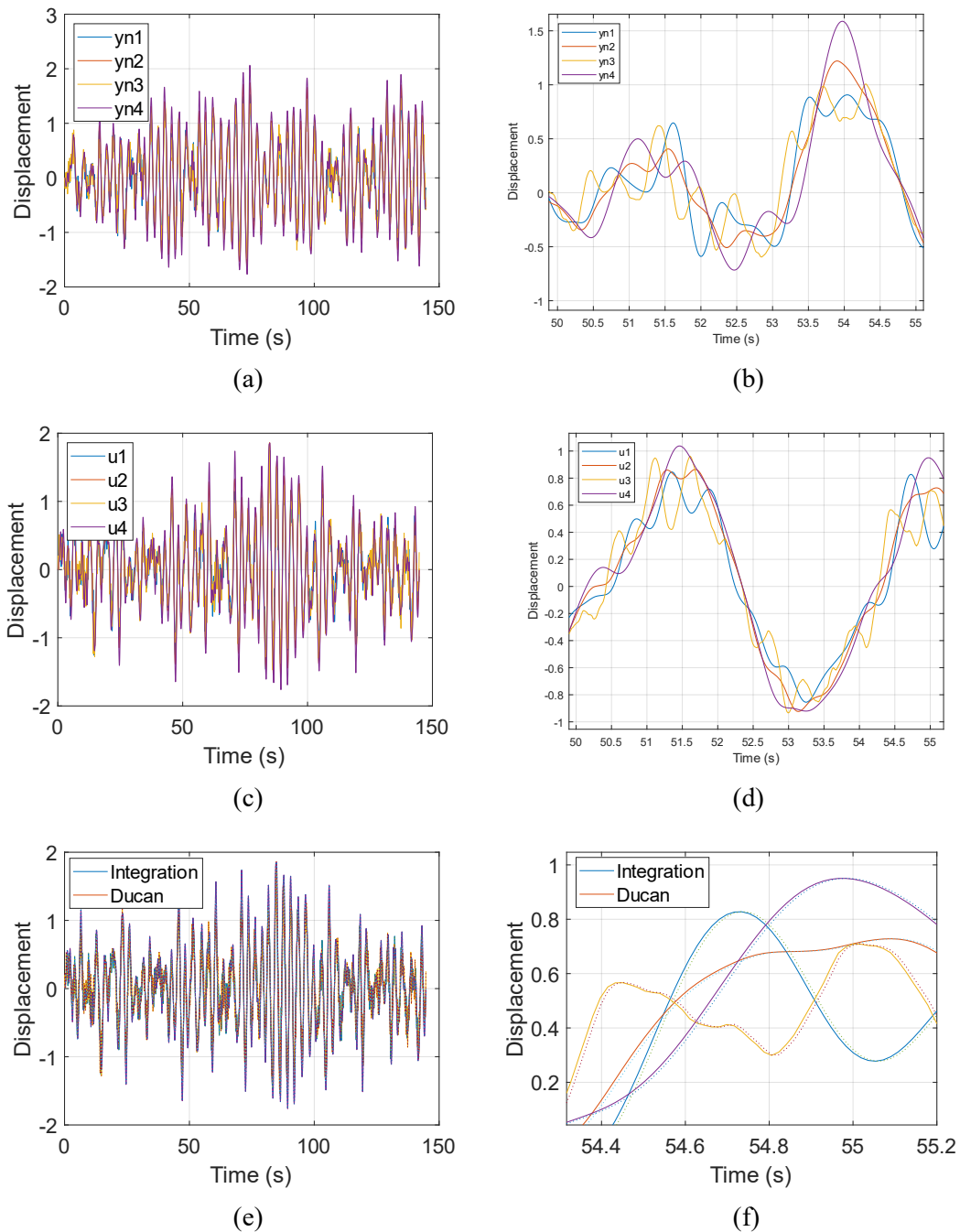
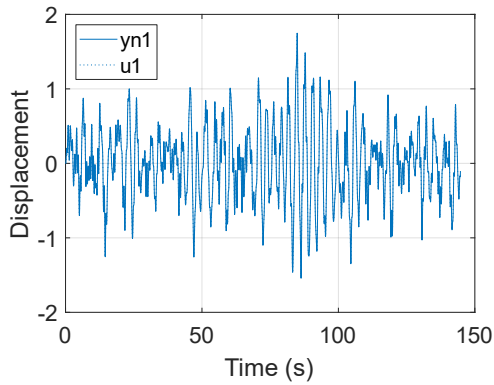
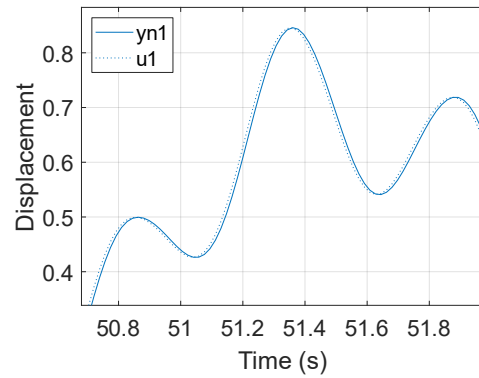


**Fig.2.1** For one random input (a) and (b) are from the discrete time linear system method, while the figure (c) and (d) are from the Duncan method. (b) is a local zoomed version of (a); (d) is a local zoomed version of (c); (e) overlapping the two methods; (f) is a local zoomed version of (e); solid line: discrete time linear system method; dash line: Duncan method.

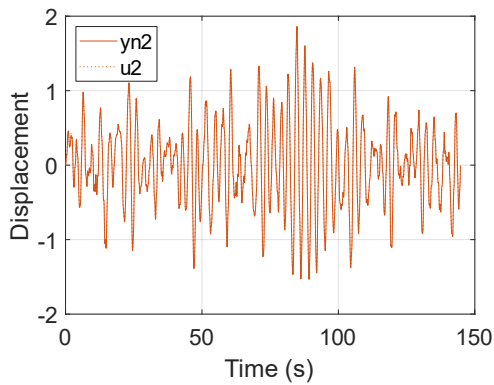
From Fig.2.1, it can be seen that two sets of signals in (a) and (c) are obtained by running **Integration.m** and **Duncan.m**. In the following analysis, we will only focus on the later part of the curve, as the system can be still unstable during the first stage and behave noisily. Specifically, to make sure the system is completely stable, we only consider the last 80% of the curve. That is to say, for the cases presented above, we will only analyze the curve behavior from 30 to 150s, neglecting the first 20%, i.e., from 0 to 30s. Each signal has 4 sets of data, because of 4-d.o.f. system. And the curves in the two figures are very similar. But after zooming in, compare to the (b), (d) have small time delay. It is more obvious in Fig.2.1 (e)(f), the curves obtained by the two methods are highly similar.



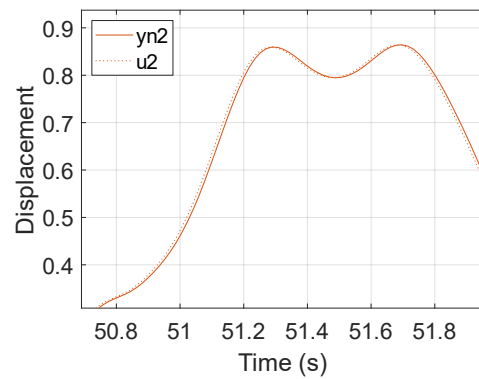
(a)



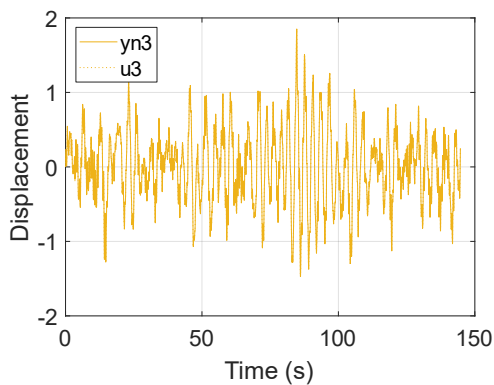
(b)



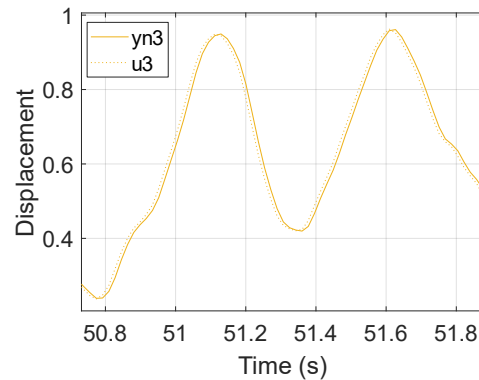
(c)



(d)



(e)



(f)

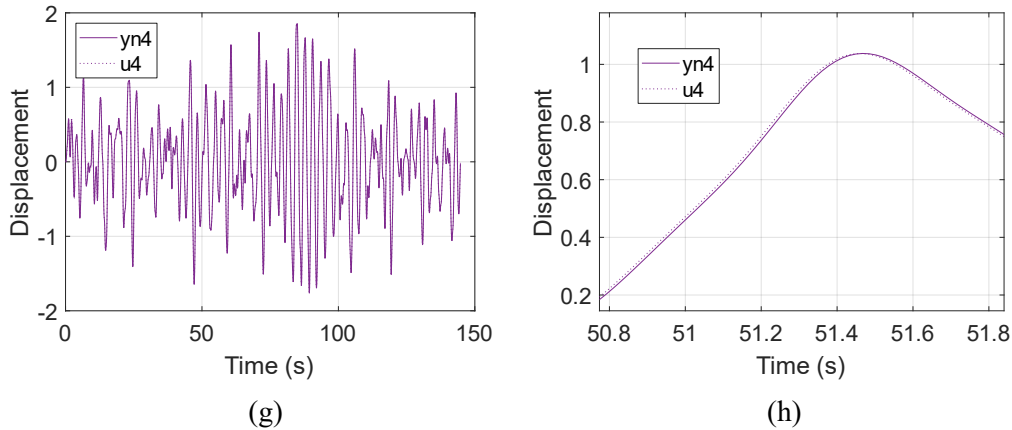


**Fig.2.2** In (a)(c)(e)(g), for one random input solid lines are from the discrete time linear system method, while dash lines are from the Duncan method; (b)(d)(f)(h) are zoomed version.

The purpose of Fig.2.2 is to separate the four sets of curves in Fig.2.1 and then compare them separately. The maximum/minimum value of (a)(c)(e)(g) around  $\pm 2$ ; and the discrete time linear system method has little delay compare to the Duncan method.

**Table 2.1** mean value and root mean square root (RMS) of the discrete time linear system method and the Duncan method

Set		1	2	3	4
Discrete time linear system method	Mean value	0.0071	0.0077	0.0087	0.0074
	RMS	0.6556	0.5754	0.4905	0.6553
Duncan method	Mean value	0.0070	0.0075	0.0086	0.0073
	RMS	0.6553	0.5750	0.4901	0.6556

The mean value of both sets of data is positive. The RMS of both sets of data is less than 1. Apart from these, the difference in the mean value between the two sets of signals is more than ten times. And the root mean square root (RMS) of the two sets of signals has an almost 20% difference.

### Case 2. Two random inputs

Considering the 4-degrees-of-freedom mechanical system that is already defined in Chapter 1, apply two random forces to the second and third mass. The MATLAB code of the forcing matrix of the discrete time linear system method is attached as following:

```
3. f=zeros(length(t),n);
4. f(:,2)=1000*randn(length(t),1); % random input on mass 2
5. f(:,3)=500*randn(length(t),1); % random input on mass 3
```

where  $t$  is the vector of time;  $n$  is the number of degrees of freedom. Then save the random input and apply it with the Duncan method. The elapsed time in **MATLAB** of the discrete time linear system method and the Duncan method is 0.27s and 0.11s. Same as case 1, It can still be



seen that the Duncan method is faster, even if the difference is small. And with such random forces, the two different methods give results as shown in Fig.2.3 and Fig.2.4.

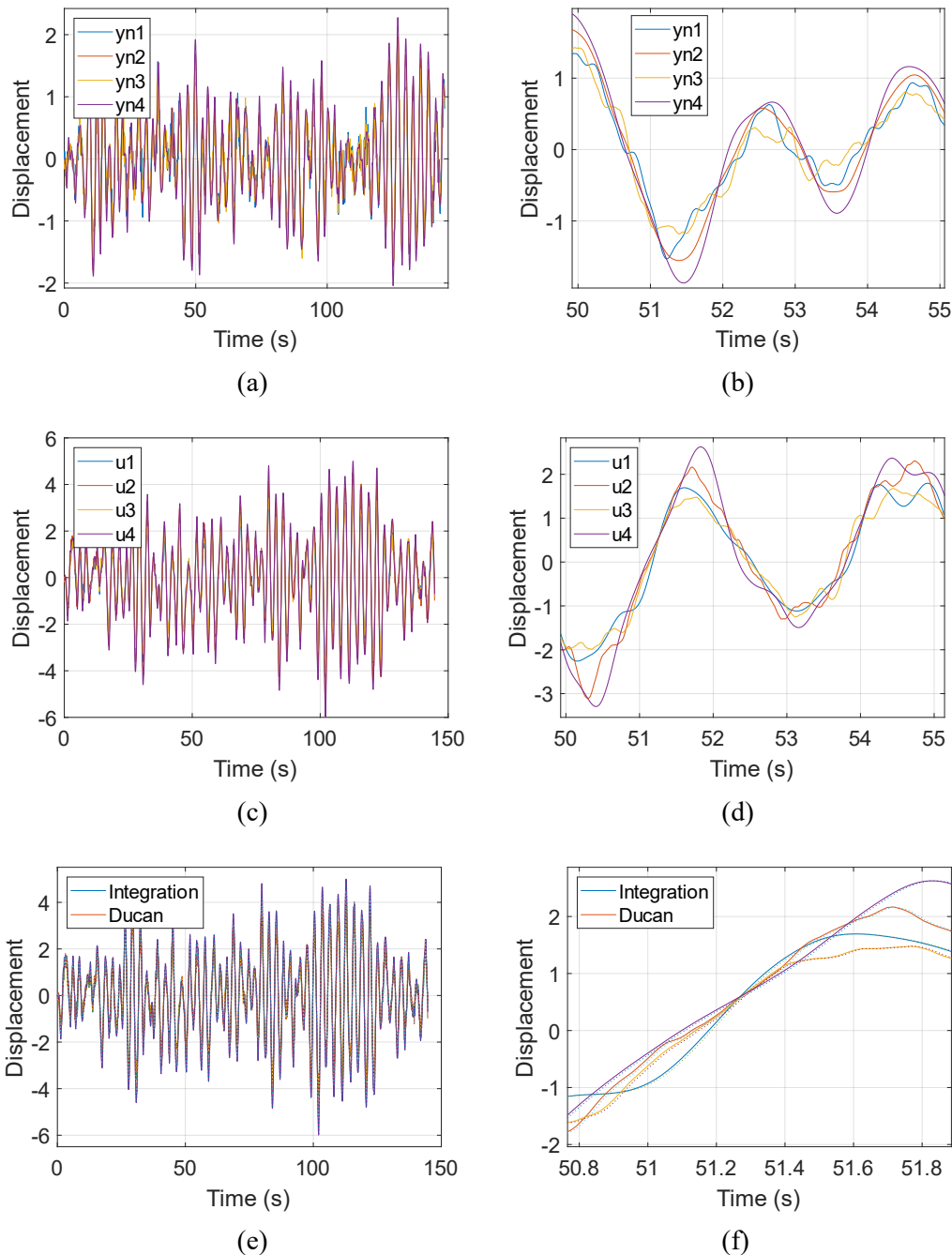
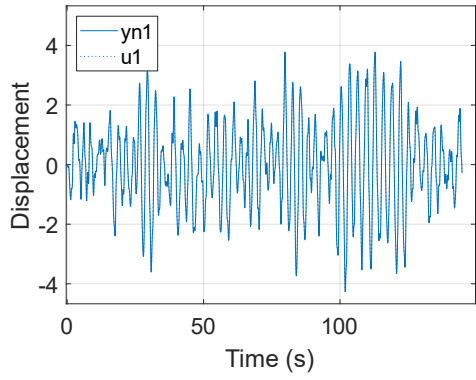
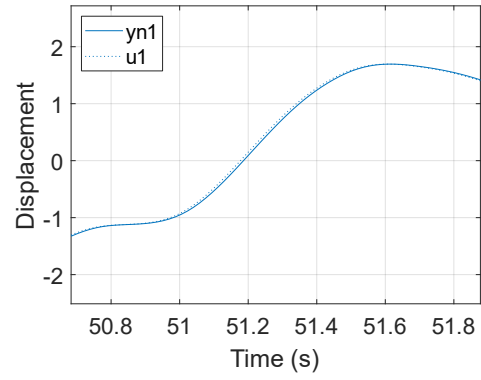


**Fig.2.3** Two random inputs (a) and (b) are from the discrete time linear system method, while figures (c) and (d) are from the Duncan method. (b) is a local zoomed version of (a); (d) is a local zoomed version of (c); (e) overlapping the two methods; (f) is a local zoomed version of (e); solid line: the discrete time linear system method; dash line: the Duncan method.

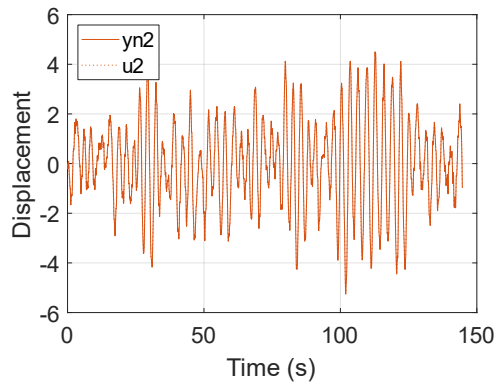
As shown in Fig.2.3, two sets of signals in (a) and (c) are obtained by running **Integration.m** and **Duncan.m**. Each signal has 4 sets of data, because of 4-d.o.f. system. As shown in Fig.2.3 (a)(c)(e), the curves in the two figures are highly similar. Even after zooming in (as shown in



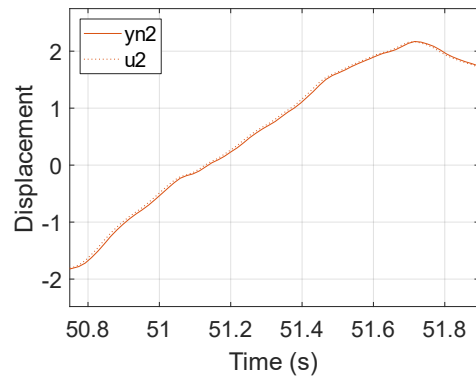
(a)



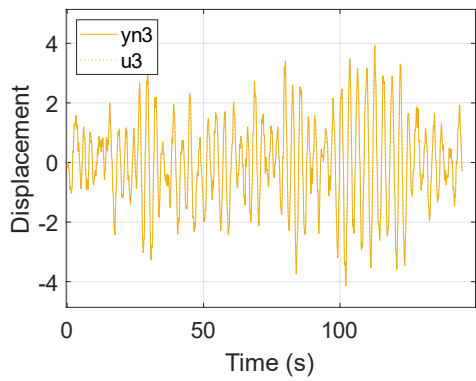
(b)



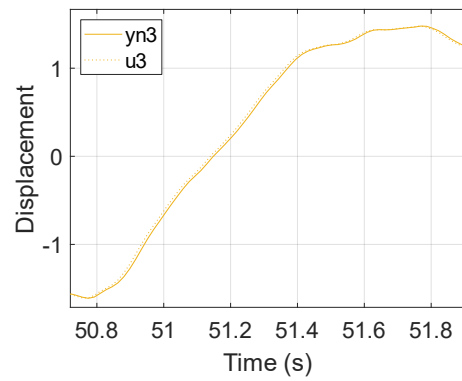
(c)



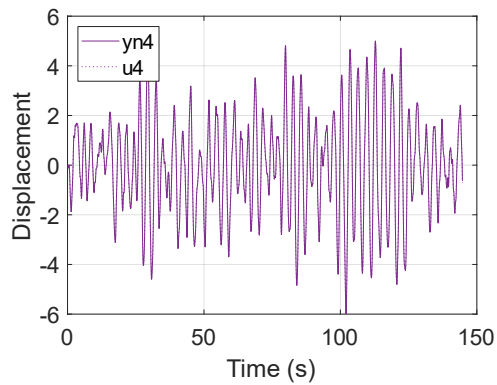
(d)



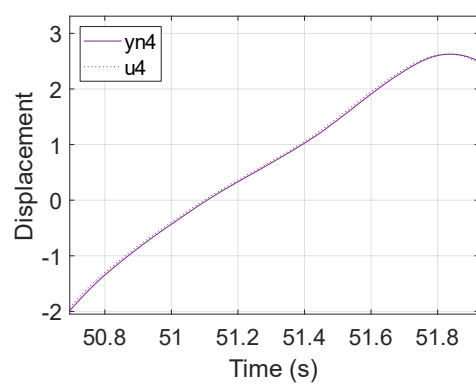
(e)



(f)



(g)



(h)

**Fig.2.4** In (a)(c)(e)(g), for one random input solid lines are from the discrete time linear system method, while dash lines are from the Duncan method; (b)(d)(f)(h) are zoomed version.

Same purpose as the last case. From Fig.2.4, the signals in (a)(c)(e)(g), the maximum/minimum value around  $\pm 4$ ; the frequency of signal in (a)(c)(e)(g) are almost same as the signal in (b)(d)(f)(h).

**Table 2.2** The mean value and the root mean square root (RMS) of discrete time linear system and Duncan method

Set		1	2	3	4
Discrete time linear system method	Mean value	-0.0065	-0.0072	-0.0080	-0.0072
	RMS	0.5998	0.5956	0.5847	0.7917
Duncan method	Mean value	-0.0064	-0.0072	-0.0080	-0.0072
	RMS	0.5996	0.6954	0.5846	0.7915

The mean value of both sets of data is negative. The RMS of both sets of data is bigger than 1 and less than 2. Apart from these, the difference in the mean value between the two sets of signals is small, nearly none. Likewise, the root mean square root (RMS) of the two sets of signals has no difference.

Case 3. One random input and one harmonic input

Considering the 4-degrees-of-freedom mechanical system that is already defined in Chapter 1, apply one random input and one harmonic input onto the third and first mass. The MATLAB code of the forcing matrix of the discrete time linear system method:

```

1. f=zeros(length(t), n);
2. f(:,1)=500*cos(2*pi*20*t)+sin(2*pi*20*2*t)+300*cos(2*pi*20*3*t)+100*sin(2*pi*20*4*t) ; % harmonic input
3. f(:,3)=500*randn(length(t),1); % random input

```

Where t is the vector of time; n is the number of degrees of freedom. Then save the random input and apply it with the Duncan method. The Elapsed time in MATLAB of the discrete time linear system method and the Duncan method is 0.244s and 0.103s. Same as before, the Duncan method is faster, even if the difference is small. And with such forces, the two different methods give results as shown in Fig.2.5 and Fig.2.6.

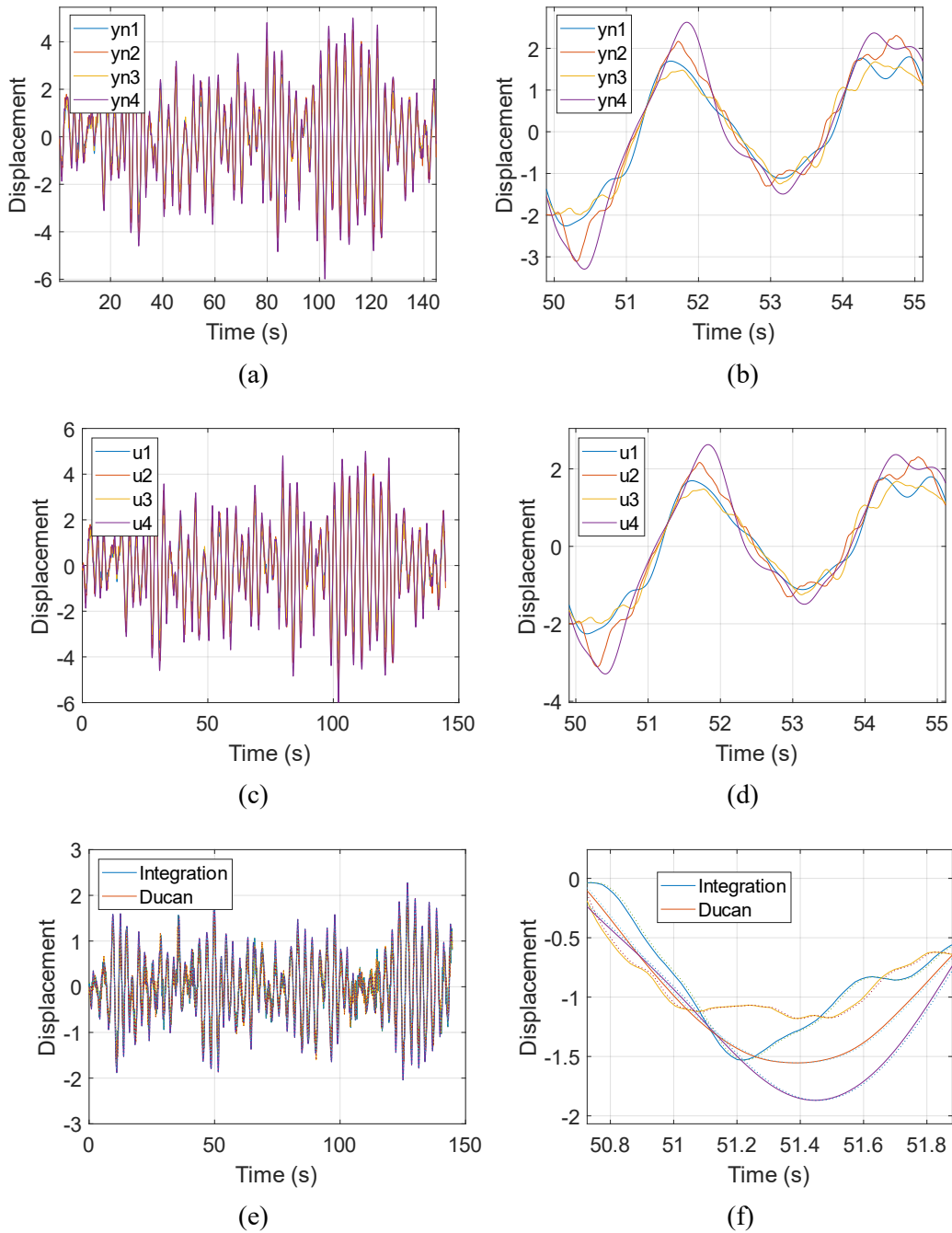
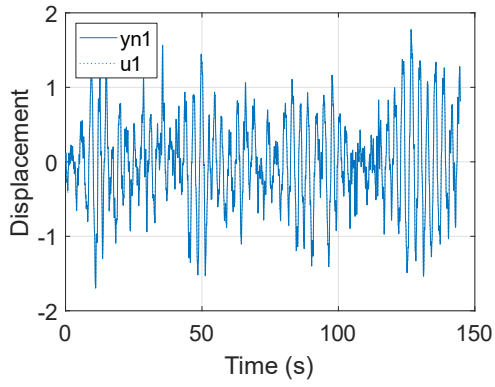
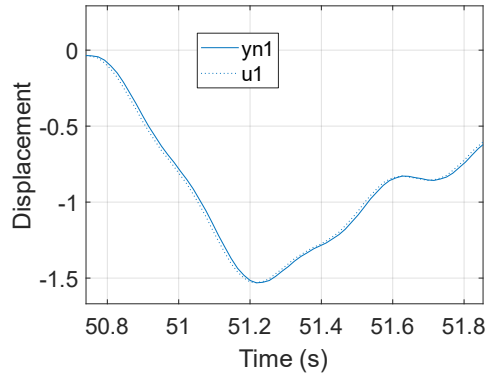


**Fig.2.5** For one random input and one harmonic input (a) and (b) are from the discrete time linear system method, while figure (c) and (d) are from the Duncan method. (b) is a local zoomed version of (a); (d) is a local zoomed version of (c); (e) overlapping the two methods (f) is a local zoomed version of (f).

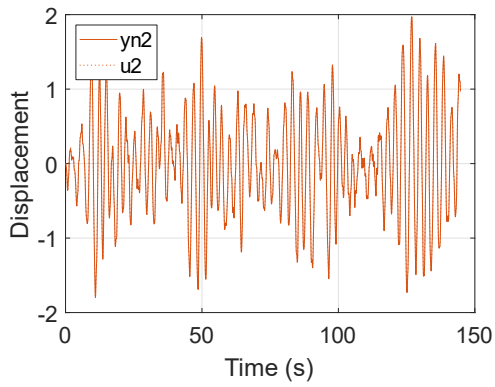
As shown in Fig.2.5, two sets of signals in (a) and (c) are obtained by running **Integration.m** and **Duncan.m**. Each signal has 4 sets of data, because of 4-d.o.f. system. As shown in Fig.2.5 (a)(c)(e), the curves are highly similar, even after zoom.



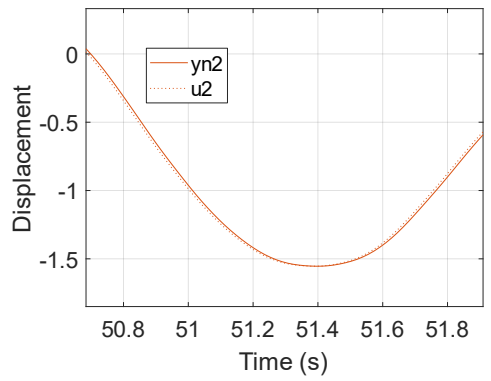
(a)



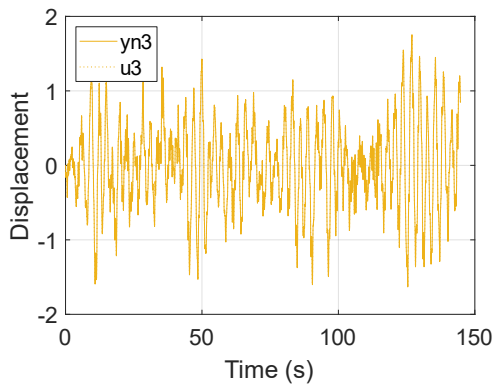
(b)



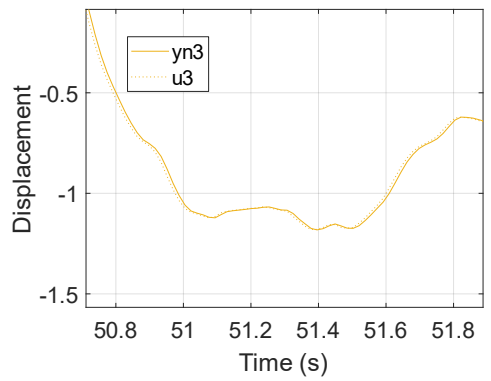
(c)



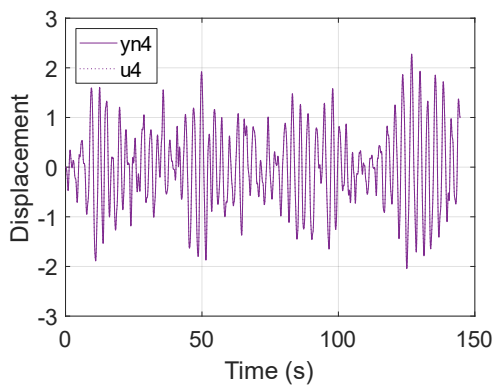
(d)



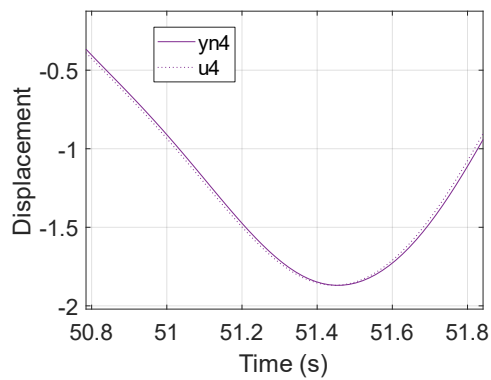
(e)



(f)



(g)



(h)

**Fig.2.6** In (a)(b)(c)(d), for one random input and one harmonic input, solid lines represent the discrete time linear system method, while dash lines represent the Duncan method; (b)(d)(f)(h) are zoomed version.

Like before from Fig.2.6, The maximum/minimum value of (a) (c) (e), and (g) around  $\pm 2$ .

**Table 2.3** The mean value and the root mean square root (RMS) of discrete time linear system and Duncan method

Set		1	2	3	4
Discrete time linear system method	Mean value	-0.0064	-0.0072	-0.0080	-0.0072
	RMS	0.5998	0.6956	0.5847	0.7917
Duncan method	Mean value	-0.0065	-0.0072	-0.0079	-0.0072
	RMS	0.5996	0.6954	0.5846	0.7915

The mean value of both sets of data is negative. The RMS of both sets of data is bigger than 1 and less than 2. Apart from these, the difference of the mean value between the two sets of signals is small, nearly none. Likewise, the root mean square root (RMS) of the two sets of signals has no difference.

In conclusion, comparing the discrete time linear system method and the Duncan method, the results obtained by the two methods are very similar. But the calculation of the Duncan method is simpler and faster to calculate.

The above three cases are based on the condition that there is no noise on measurements. But if we add 5% of noise on the measurements, the result for the first case (with one random input) is obtained as shown in Fig.2.7:

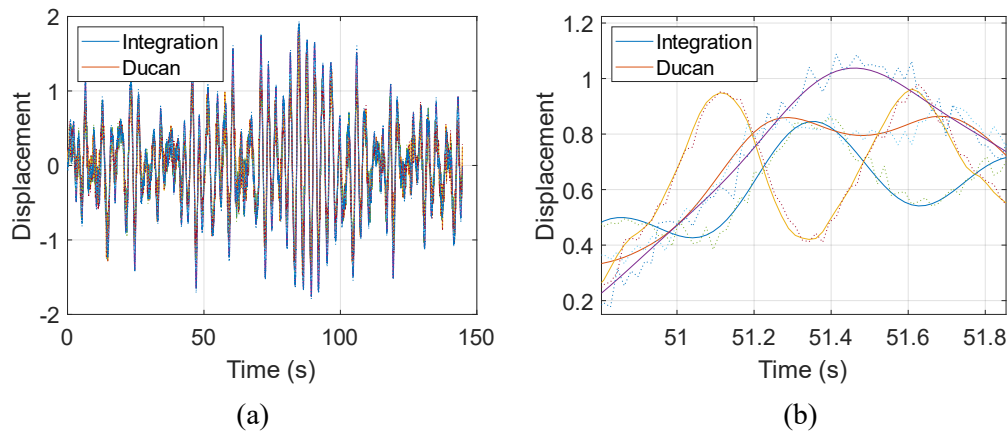


**Fig.2.7** For one random input (a)overlapping the two methods(b)is a local zoomed version of (a). solid line: discrete time linear system method; dash line: Duncan method.

It can be seen from Fig.2.7 that the results obtained by the Duncan method are less stable than the discrete time linear system.

# Chapter 3 - Comparison of modal parameters extraction methods

In this part, we will compare the input-output and output-only methods for extracting the modal parameters in the case of only one random input. Input-output method indicates those modal parameters estimation methods that need both inputs and outputs of a system, while the output-only methods are those where the system inputs are not needed and the estimation process can be done with only outputs. Both of them are performed through a simple modal parameter estimation method in the frequency or Z-domain, namely LIPEZ, which can work in both cases of input-output or output-only.

Furthermore, the comparison is performed in an example case of a 7-degrees-of-freedom mechanical system, whose third mass (mass-3) is excited, owing the modal properties in Table 3.1.

**Table 3.1 Modal parameters of a 7-degrees-of-freedom mechanical system**

	Mode 1	Mode 2	Mode 3	Mode 4	Mode 5	Mode 6	Mode 7
<b>Natural frequency (Hz)</b>	8.09	24.70	35.32	45.03	47.55	53.46	65.99
<b>Damping ratio (%)</b>	0.22	1.44	1.43	1.15	1.38	1.61	1.97

With these modal parameters, we can easily obtain its modal matrix as Table 3.2.

**Table 3.2 Modal matrix of the mechanical system presented in Table 3.1**

Mode 1	Mode 2	Mode 3	Mode 4	Mode 5	Mode 6	Mode 7
0.5128 - 0.0006i	0.7977 + 0.0039i	2.2427 - 0.0263i	-1.5912 - 1.1860i	7.4538 + 0.4177i	-0.4630 + 0.0208i	-0.2626 + 0.0099i
0.9844 + 0.0002i	1.3355 + 0.0038i	3.0865 - 0.1198i	-1.8243 - 0.2038i	-4.1329 - 0.3381i	-0.6792 + 0.0065i	-0.1024 - 0.0039i
1.0000	1.0000	1.0000	1.0000	1.0000	1.0000	1.0000
1.1644 - 0.0006i	0.7532 + 0.0075i	-2.5286 + 0.1060i	9.8243 + 2.5085i	0.3269 + 0.3887i	-0.4436 + 0.0249i	-0.1128 + 0.0086i
1.1441 - 0.0000i	0.4227 - 0.0214i	-0.4809 + 0.0108i	-2.4157 - 0.5334i	-0.5139 - 0.1086i	1.3785 - 0.0568i	-0.8201 - 0.0298i
1.2519 - 0.0008i	-0.3743 - 0.0075i	-3.0708 + 0.0159i	-8.6309 - 2.0115i	0.2343 - 0.1948i	-0.5198 + 0.0182i	0.2128 + 0.0053i
1.3562 - 0.0020i	-2.9840 + 0.0012i	2.2769 - 0.0218i	2.9705 + 0.7310i	0.0045 + 0.0740i	-0.0331 - 0.0184i	0.0222 + 0.0097i

These modal parameters and modes can be seen as the right answer. And will be compared to the extracted modal parameters, in the input-output and output-only cases by using the LIPEZ

method. LIPEZ is a model parameter estimation method in the frequency domain [2]. This approach, which can work for multi-input-multi-output (MIMO) and output-only problems, provides a procedure to largely reduce the problem dimensions when dealing with the large data sets (i.e.,  $N_{FRF} \gg 1$ , where  $N_{FRF}$  is the number of FRFs).

For a n-degree of freedom linear and time-invariant system the z-transformed impulse response function (with sampling frequency  $f_s$ ) is:

$$H_k = \sum_{r=1}^{2n} A_r \frac{z_k}{z_k - z_r} = \frac{b_1 z_k + \dots + b_{2n} z_k^{2n}}{a_0 + a_1 z_k + \dots + a_{2n-1} z_k^{2n-1} + z_k^{2n}}$$

It has in total  $4n$  unknown real parameters, i.e.,  $\mathbf{a} = a_0, a_1, \dots, a_{2n-1}$  and  $\mathbf{b} = b_1, b_2, \dots, b_{2n}$ . To solve for these unknowns, the LIPEZ method does not need to apply the Least-square method  $N_{FRF}$  times. Instead, it only needs to apply the Least-square method once by introducing a positive real scalar  $E$ , which is defined as the overall sum of the square of the errors between the measured and true FRFs:

$$E = \sum_{m=1}^{N_{FRF}} \mathbf{e}_m^H \mathbf{e} = \text{Re} \sum_{m=1}^{N_{FRF}} [(\mathbf{A}_m \mathbf{a} - \mathbf{B} \mathbf{b}_m - \mathbf{w}_m)^H (\mathbf{A}_m \mathbf{a} - \mathbf{B} \mathbf{b}_m - \mathbf{w}_m)]$$

where all the symbols' physical meanings can be found in [2] if not specifically stated. To minimize  $E$ , which is a function of  $\mathbf{a}$  and  $\mathbf{b}_m$ , where  $m$  indicates the  $m$ -th FRF, we can set the corresponding derivative of  $E$  to null as follows:

$$\begin{cases} \frac{\partial E}{\partial \mathbf{a}} = 0 \\ \frac{\partial E}{\partial \mathbf{b}_m} = 0 \end{cases}$$

As the dimension of  $\frac{\partial E}{\partial \mathbf{a}}$  is  $2n \times 2n$  and the second sub-equation above ( $\frac{\partial E}{\partial \mathbf{b}_m} = 0$ ) can be substitute in the first one, the problem dimension is dropped to  $2n$  by using LIPEZ method, compared to the normal Least-square method. All the details can be seen in [2].

### 3.1 Input-Output Method

Herein, the LIPEZ method is implemented elaborating the frequency response functions (FRFs) of a single input and multiple outputs (SIMO) system.

The time histories of a single input (a time-varying force acting on the third mass) and 7 outputs (resultant displacements of seven masses) are supposed to be given, either numerically or experimentally.

First, we need to obtain the FRF based on the input and output time histories. It is done by the Fast Fourier Transform (FFT). However, the result varies with its number of samples ( $N_{FFT}$ )



Therefore, to have the suitable FRF, we change the  $N_{\text{FFT}}$  and plot the obtained FRFs. The results are attached in Fig. 3.1, where (a), (b), and (c) indicate  $N_{\text{FFT}} = 2^{12}$ ,  $2^{14}$ , and  $2^{16}$  respectively with sampling frequency  $f_s = 512 \text{ Hz} = 2^9 \text{ Hz}$ .

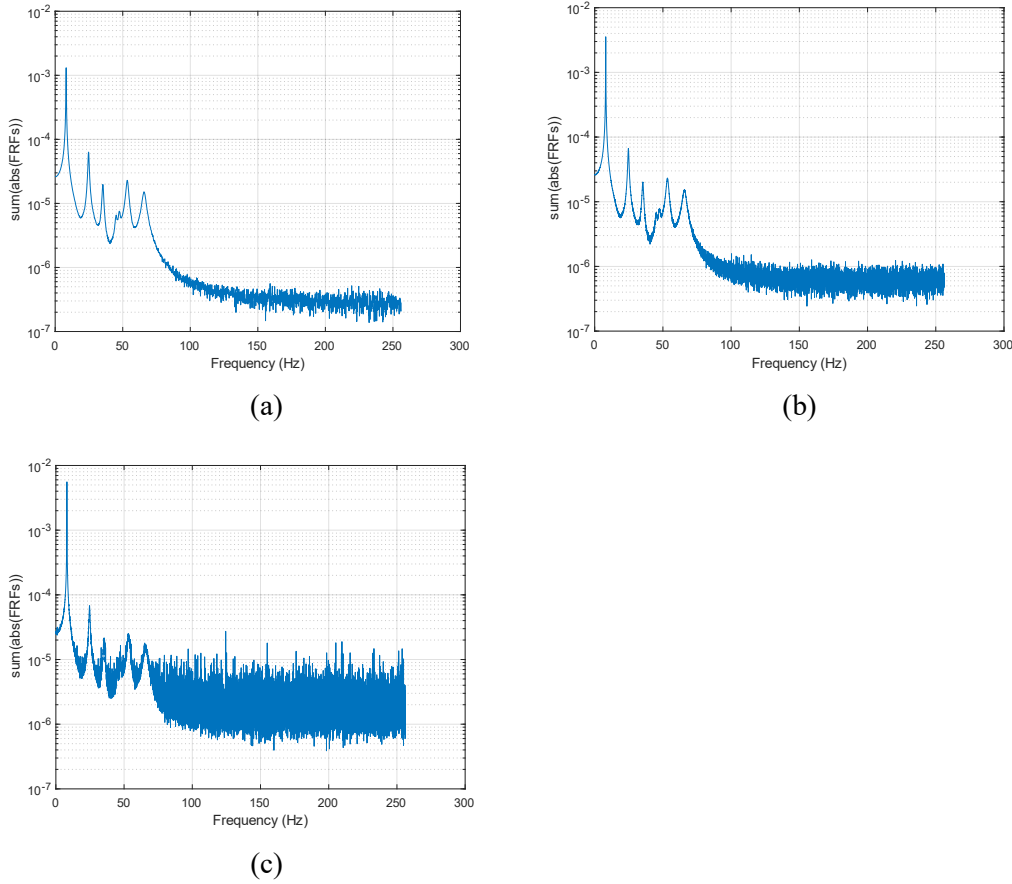


**Fig.3.1.2** FRFs obtained from Fast Fourier Transform (FFT) onto the input and output time histories with different number of FFT, where (a)  $N_{\text{FFT}} = 2^{12}$ , (b)  $N_{\text{FFT}} = 2^{14}$ , and (c)  $N_{\text{FFT}} = 2^{16}$ .

As seen,  $N_{\text{FFT}} = 2^{12}$ ,  $2^{14}$ , and  $2^{16}$  give similar results between 0 and 100Hz. Generally, we don't start from 0Hz, because FRFs may not express well at 0Hz, but not in this case. There are 7 distinct peaks, even though it can be seen heavier noise for larger  $N_{\text{FFT}}$ , especially for higher frequency band beyond 100Hz. Therefore, we study the frequency range of 0-100Hz, which is the most suitable. In such way, in the following numerical experiments we take  $N_{\text{FFT}}=2^{14}$  and only consider 0-100Hz frequency range for comparison and analysis.

Hereafter, the model order should be determined. This can be done by running the **LIPEZ.m** function with different mode numbers ( $n$ ) within 0-100Hz. The suitable value of the mode number can be chosen depending on the obtained results that will be discussed below. Here in this example, three different mode numbers, i.e.,  $n = 30$ , 50 and 100, are tried and the results can be seen in Fig.3.1.3 (the example with  $n=100$  contains also  $n=30$  and  $n=50$ . So, we only keep the result with  $n=100$ ). The running times are 38.3s, 105.6s and 554.7s. This means that the larger the mode number, the more time it takes.

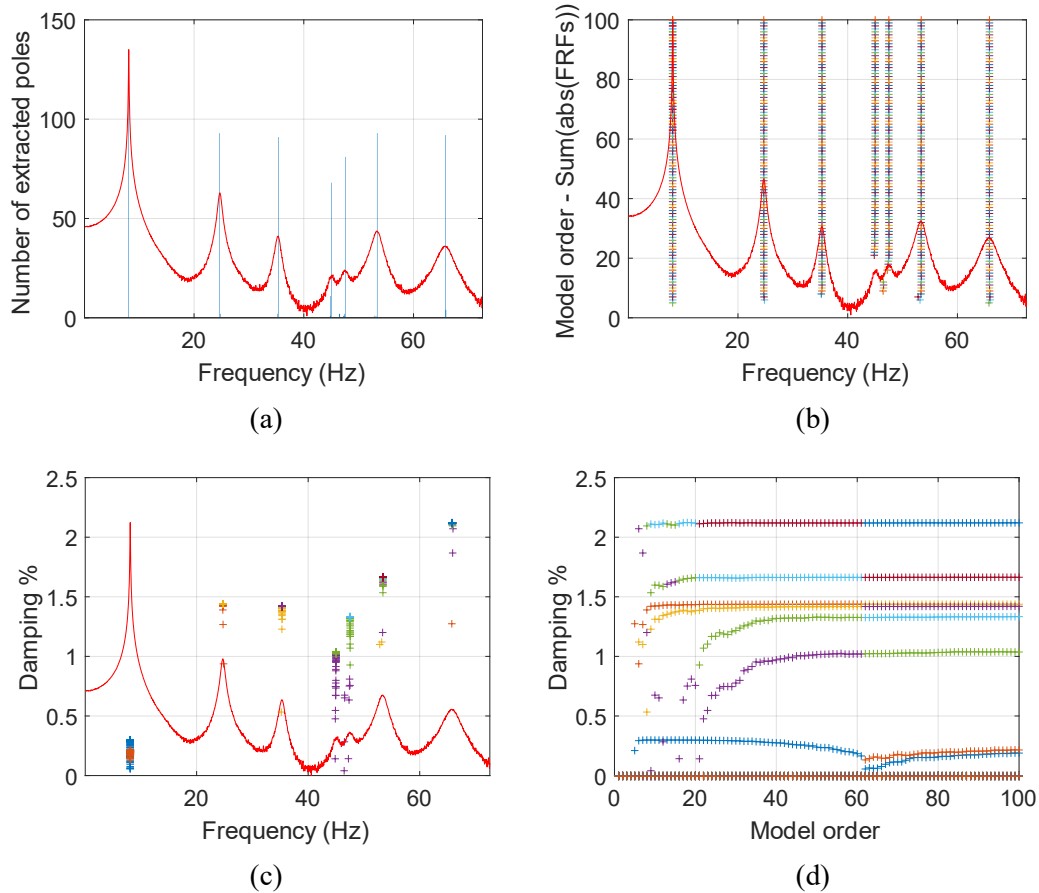


**Fig.3.1.3** (a) Histogram of all the extracted frequencies, overlaid on the sum of the modulus of all the FRFs. (b) The frequencies extracted with an increasing model order overlaid on the sum of the moduli of all the FRFs with a model order of 100. (c) Damping ratios as a function of the frequencies overlaid on the sum of the moduli of all the FRFs with model order of 100. (d) The damping ratios extracted with model order of 100.

As can be seen from Fig.3.1.3 (a), there are 7 peaks located at 8.1, 24.5, 35, 45, 47.5, 55, and 65Hz, respectively. Fig.3.1.3 (b) to (d) are beneficial to understand which modes are stable, whose frequencies are quickly detected and damping ratio is much more valuable. In Fig.3.1.3 (b) it can be seen that the fourth and fifth peaks located at 45 and 47.5Hz, respectively, are not as quickly detected as the others, and they do not appear when the mode number is lower than 20.

And in Fig.3.1.3 (c)(d), we can find that when the mode number increases, the damping ratios approach their corresponding constant values. In this way,  $n = 100$  certainly gives the best result. However, it has also the highest time consumption among the three. Furthermore, we can find from Fig.3.1.3 (c)(d) that the corresponding natural frequency and the damping ratio of the seven peaks are respectively 8.1Hz and 0.3%, 24.5Hz and 1.43%, 35Hz and 1.4%, 45Hz and 0.78%, 47.5Hz and 1.2%, 55Hz and 1.6%, and 65Hz and 2.1%. Basically, they are exactly the same as the data given in Table 3.3. Therefore, considering the balance between the result and time expense,  $n = 50$  seems to be a good choice.

### Definition of the correct modal parameters

This section aims to describe how the ‘best’ modal parameters can be selected among the set of extracted modes. As we already obtained the natural frequencies and damping ratios, here we need to check if they are stable. At the same time, their corresponding mode shapes are compared through MAC.

For natural frequency stabilization, we compare the relative change between two consequent frequencies that can be written in the form:

$$\Delta f = \frac{f_i^m - f_i^{m-1}}{f_i^m}, m = 1, 2, \dots, n \quad (3.1)$$

If  $\Delta f < 0.5\%$  is satisfied, we regard the corresponding  $f_i^m$  in plot (for example: Fig.3.1.4 (b)) as a stable point and mark it as “O”, otherwise it is treated as unstable and marked as “X”.

For the damping stabilization, we compare the relative change between two consequent damping ratio that can be written in the form:

$$\frac{\xi_i^m - \xi_i^{m-1}}{\xi_i^m} = \Delta \xi, m = 1, 2, \dots, n \quad (3.2)$$

If  $\Delta \xi < 5\%$  is satisfied, we regard  $\xi_i^m$  in plot (for example: Fig.3.1.4 (c) and (d)) as a stable point and mark it as “Δ”.

For mode shape stabilization, we compare the relative change between two consequent mode shape with MAC that can be written in the form:

$$\text{MAC}(\{\psi\}_i^m, \{\psi\}_i^{m-1}) = \frac{|\{\psi\}_i^{m*} \{\psi\}_i^{m-1}|^2}{\|\{\psi\}_i^m\| \|\{\psi\}_i^{m-1}\|} \quad (3.3)$$

Where \* designates the conjugate transpose of a complex vector. MAC, namely Modal Assurance Criterion, is a commonly-used statistical indicator to the similarity between mode shapes [5]. Its value is bounded between 0 and 1. The closer to 1 the value of MAC between two mode shapes is, the stronger the similarity between them exists. In the contrast, the closer to 0 the value of MAC, the more different the two mode shapes are [5]. Further details on MAC can be found in [5].

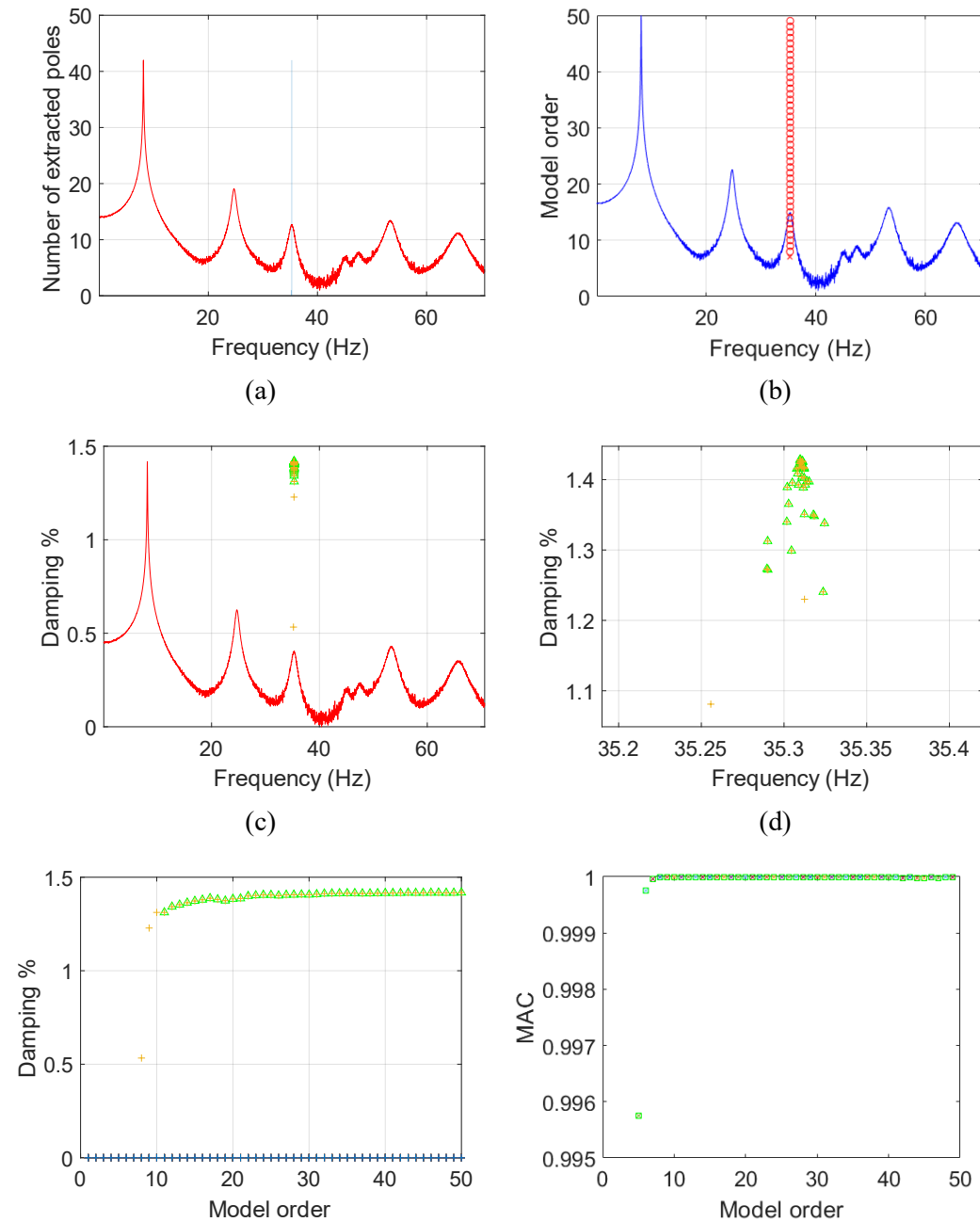
Here we set the threshold of MAC as 95%, i.e., we regard  $\{\psi\}_i^m$  in plot (for example: Fig.3.1.4 (e)) as a stable point and mark it as “□” if its  $\text{MAC} > 95\%$ .

Furthermore, an extended version of the MAC, which is valid for all kinds of vectors, is also calculated. Its expression is as follows according to [6]:

$$\text{MACX}(\{\psi\}_i^m, \{\psi\}_i^{m-1}) = \frac{(|\{\psi\}_i^{m*} \{\psi\}_i^{m-1}| + |\{\psi\}_i^{mT} \{\psi\}_i^{m-1}|)^2}{(\{\psi\}_i^{m*} \{\psi\}_i^m + |\{\psi\}_i^{mT} \{\psi\}_i^m|)(\{\psi\}_i^{m-1*} \{\psi\}_i^{m-1} + |\{\psi\}_i^{mT} \{\psi\}_i^{m-1}|)} \quad (3.4)$$

The results of the above formulas are shown beyond Fig.3.1.3. In this case, we can set 0-10Hz, 20-30Hz, 30-40Hz, 44-46Hz, 47-48Hz, 50-60Hz, and 60-70Hz as Mode 1, Mode 2, Mode 3, Mode 4, Mode 5, Mode 6, and Mode 7 to compare the original natural natural frequency, damping ratio and modal matrix in Table.3.1 and Table3.2. For reasons of space, we only discuss the ‘good’ case and the ‘worst’ case here (it is a better case if the result is closer to the ideal modal parameters). In this case, that are Mode 3 and Mode 4.

**Mode 3: 30-40Hz frequency range with NFFT=2<sup>14</sup>, n=50**



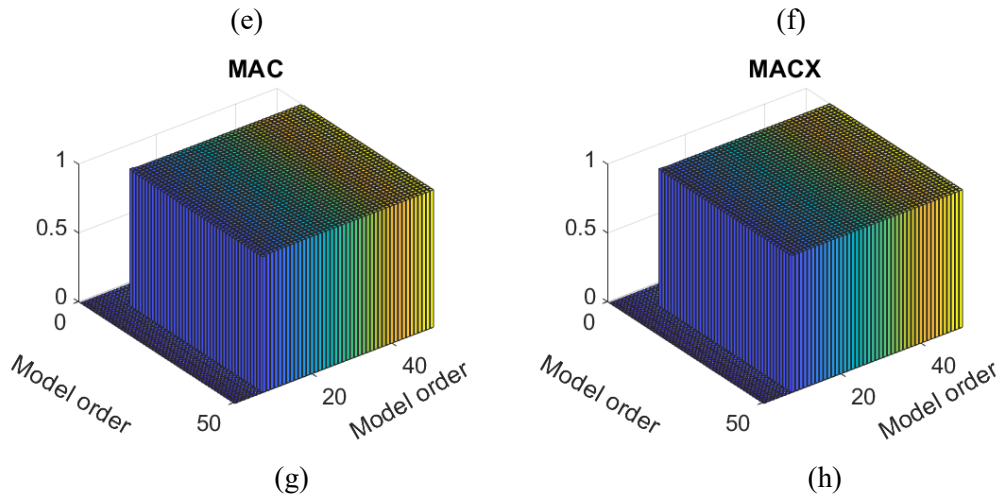


**Fig.3.1.4** (a)(b)(c)(e) have same meaning with Fig.3.1.3 in addition to including stabilized images.(d) is the zoom of (c). (g) and (h) represent MAC and MACX of this system.

Except for the first point in Fig.3.1.4 (b), the others are stable points. We can read from this figure that the natural frequency of Mode 3 is 35.3Hz. Fig.3.1.4 (c) is not good to read so it is locally enlarged, as shown in Fig.3.1.4 (d). It can be seen that the damping ratio of the Mode 3 is located around 1.43%. From the previous section, we know that as the mode number increases, the damping ratio tends to stable at a fixed value. Fig.3.1.4 (e) indicates similar trend.

Fig.3.1.4 (f) is the result of MAC between the mode shapes, where the MAC number between the mode shape of each mode order and of the next mode order is calculated. According to the physical meaning of the MAC values stated above, it can be seen from this figure that the mode shape of Mode 3 is stable and similar as almost all their MAC numbers are close to 1.

Fig.3.1.4 (g)(h) present the results of calculated MAC and MACX numbers between the mode shape of each mode order and the mode shape of all other mode orders including themselves. As can be seen from these two figures, except those cases with relatively small mode order, where no valid value of MAC and MACX presents as Mode 3 was not detected at this region, most of the results are quite close to 1. It demonstrates that these mode shapes are highly similar.

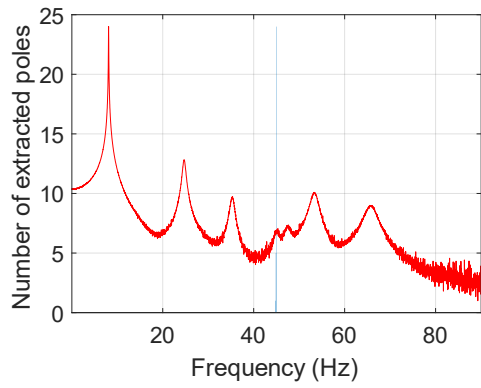
**Table 3.3** Mode shape of 30-40Hz frequency range with NFFT=2<sup>14</sup>, n=50

	Mode 1	Mode 2	Mode 3	Mode 4	Mode 5	Mode 6	Mode 7
<b>Mode shape</b>	2.4984 - 0.1575i	3.3495- 0.0708i	1.0000+ 0.0000i	-2.7580- 0.0179i	-0.4987+ 0.0335i	-3.3046 +0.2650i	2.4703 - 0.1406i

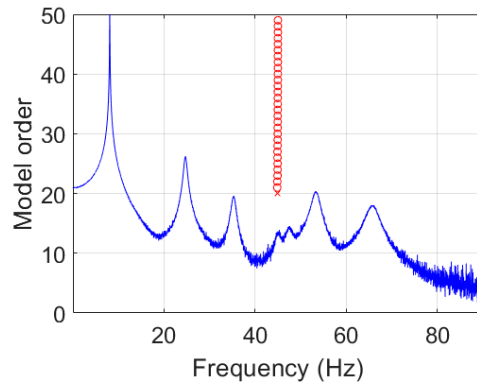
Therefore, we can read out from Fig.3.1.4 that the natural frequency and stable damping ratio are 35.3Hz and 1.43%. Compared to the corresponding values listed in Table 3.1 for the Mode 3, it can be seen that the error is smaller than 1%. Furthermore, it is worthy mentioning that the value of MAC number using the data provided in Table.3.3 and Table 3.1 for Mode 3 is 0.997. All of these suggests a very good agreement between the estimation from LIPEZ method with

respect to the actual modal parameters.

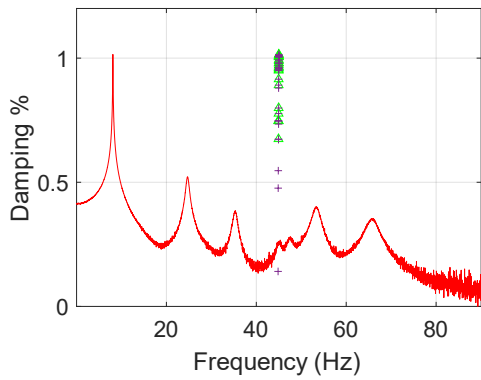
**Mode 4: 44-46Hz frequency range with NFFT=2<sup>14</sup>, n=50**



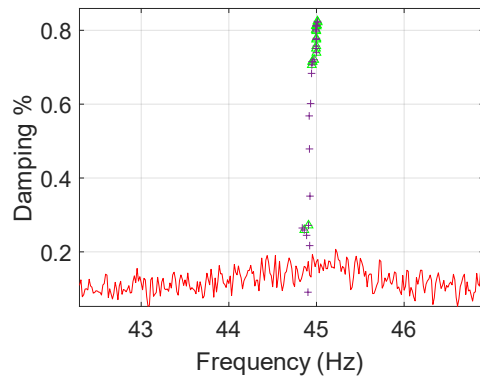
(a)



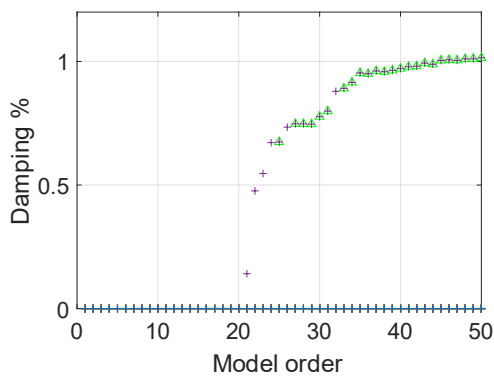
(b)



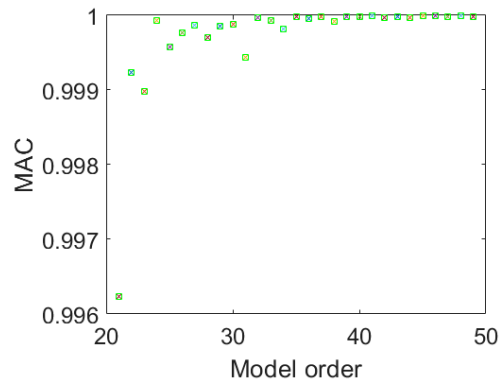
(c)



(d)



(e)



(f)

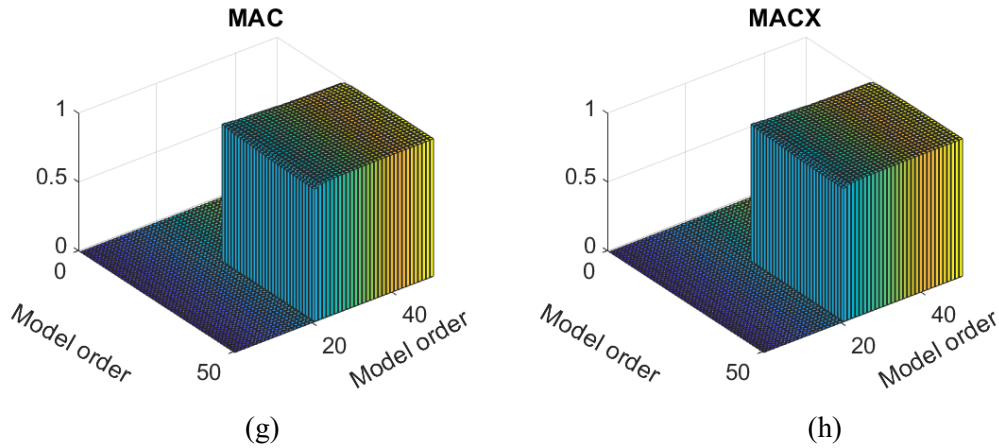


**Fig.3.1.5** (a)(b)(c)(e) have same meaning with Fig.3.1.3 in addition to including stabilized images.(d) is the zoom of (c). (g) and (h) represent MAC and MACX of this system.

Similarly, we can read from Fig.3.1.5 (b)(c)(d)(e) that the natural frequency and the damping ratio of Mode 4 are 45Hz and 0.82%, respectively. The errors are 0 and 28.7% compared to the corresponding values provided in Table 3.1 for Mode 4. And it can be seen from Fig.3.1.5 (f) that all the MAC number is close to 1, meaning that the mode shape of Mode 4 is stable and similar. All the valuable number in Fig.3.1.5 (g)(h) are close to 1, which means that these mode shapes are highly similar.

**Table 3.4** Mode shape of 44-46Hz frequency range with NFFT=2<sup>14</sup>, n=50

	<b>Mode 1</b>	<b>Mode 2</b>	<b>Mode 3</b>	<b>Mode 4</b>	<b>Mode 5</b>	<b>Mode 6</b>	<b>Mode 7</b>
<b>Mode shape</b>	0.5558 + 5.1688i	-1.8134 + 8.9897i	1.0000 + 0.0000i	8.2765 - 39.4596i	-1.5969 + 8.9927i	-8.0255 +33.8346i	3.0176 - 11.6629i

Furthermore, the MAC value based on Table.3.4 and Table 3.1 Mode 4 is calculated as 0.98, approximately 1. All of these prove that the LIPEZ method gives accurate estimations of the modal parameters except damping ratio for Mode 4.

In conclusion, when dealing with the input-output cases, the LIPEZ method gives highly accurate natural frequency estimation, which is almost the same of the actual value, and fairly good mode shapes estimation, while insufficiently reliable damping ratios may occur.

### 3.2 Output-Only

Normally, we calculate the FRFs by calculating the ratio between the Fourier transform of the output and of the input time history. However, in the output-only case, there is no data on input, i.e., we can only use the output data to estimate the modal parameter. Therefore, the original way is no longer applicable. Here, the ODS method reported in [7] is used. ODS, namely Operating Deflection Shapes or Operating Mode Shapes, is a method applicable in output-only cases. It can be obtained from the output-only data of two or more DOFs of a system.

And to obtain the ODS, the CPSD (cross power spectrum density) between the two responses is needed first. According to [7], the CPSD is calculated as follows:

$$G_{xy}(\omega) = F_x(\omega)F_y^*(\omega) \quad (3.5)$$

where  $G_{xy}(\omega)$  is the CPSD between DOF-x and DOF-y,  $F_x(\omega)$  and  $F_y(\omega)$  are respectively the Fourier transform of the roving and the (fixed) reference responses, and \* means complex conjugate.

Replacing x in y of equation (3.5),  $G_{yy}(\omega)$ , the auto spectrum of the reference response, is obtained. Similarly, the auto spectrum of the roving response,  $G_{xx}(\omega)$ , can be obtained by replacing y in x.

Hereafter, the ODS FRF can be calculated with only output data as follows [7]:

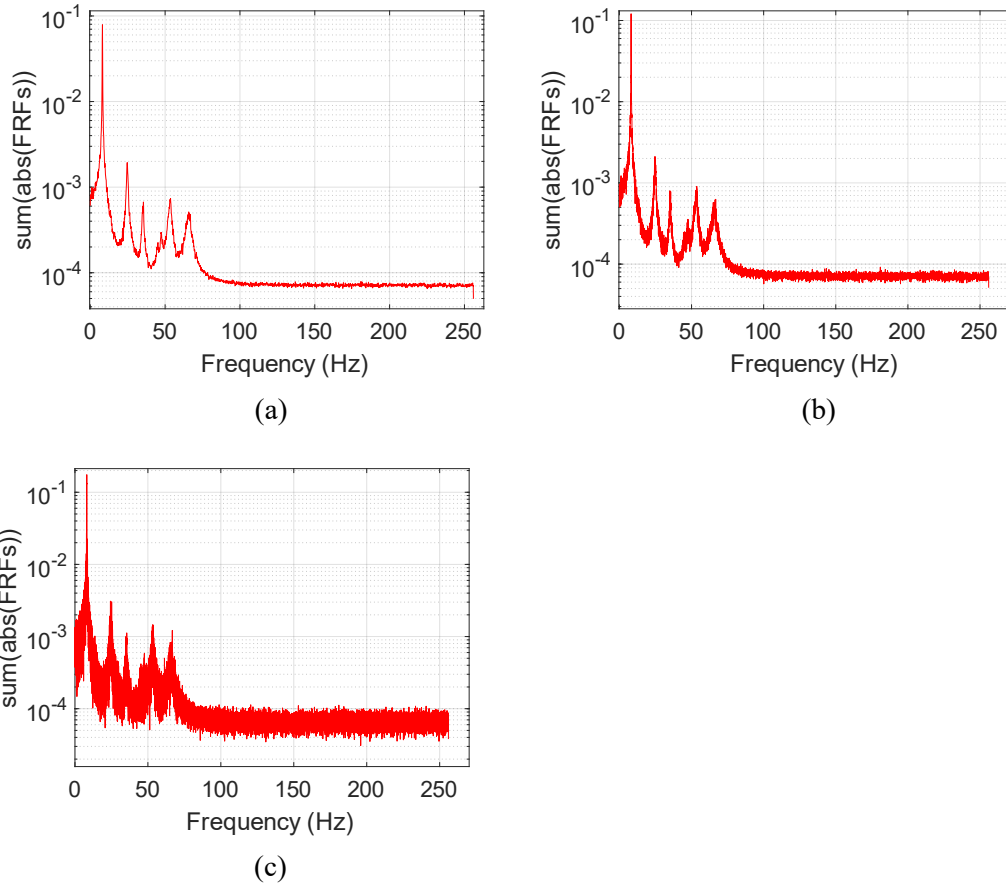
$$\text{ODS FRF}(\omega) = \sqrt{G_{xx}(\omega)} \frac{G_{xy}(\omega)}{|G_{xy}(\omega)|} \quad (3.6)$$

#### 3.2.1 ODS (Operating Deflection Shapes or Operating Mode Shapes)

In this section we discuss the procedure with the same example as before: a 7-DOF mechanical system, whose third mass (mass-3) is excited. First, the ODS FRF is computed only based on the output time histories according to equation (3.5) and (3.6). Here we set the last point (Point 7) as the reference. It can be selected from the seven points freely as long as it is not still, which would give a null  $F_y(\omega)$  [7].

However, during the numerical experiments, it is found that the result varies with the number of samples ( $N_{\text{FFT}}$ ). Therefore, the  $N_{\text{FFT}}$  is adjusted to have suitable OSD FRF (the obtained ODS FRFs is plotted every time to help to select proper  $N_{\text{FFT}}$ ). The results are attached in Fig.3.2.1, where (a), (b), and (c) indicate  $N_{\text{FFT}} = 2^{12}$ ,  $2^{14}$ , and  $2^{16}$  respectively.

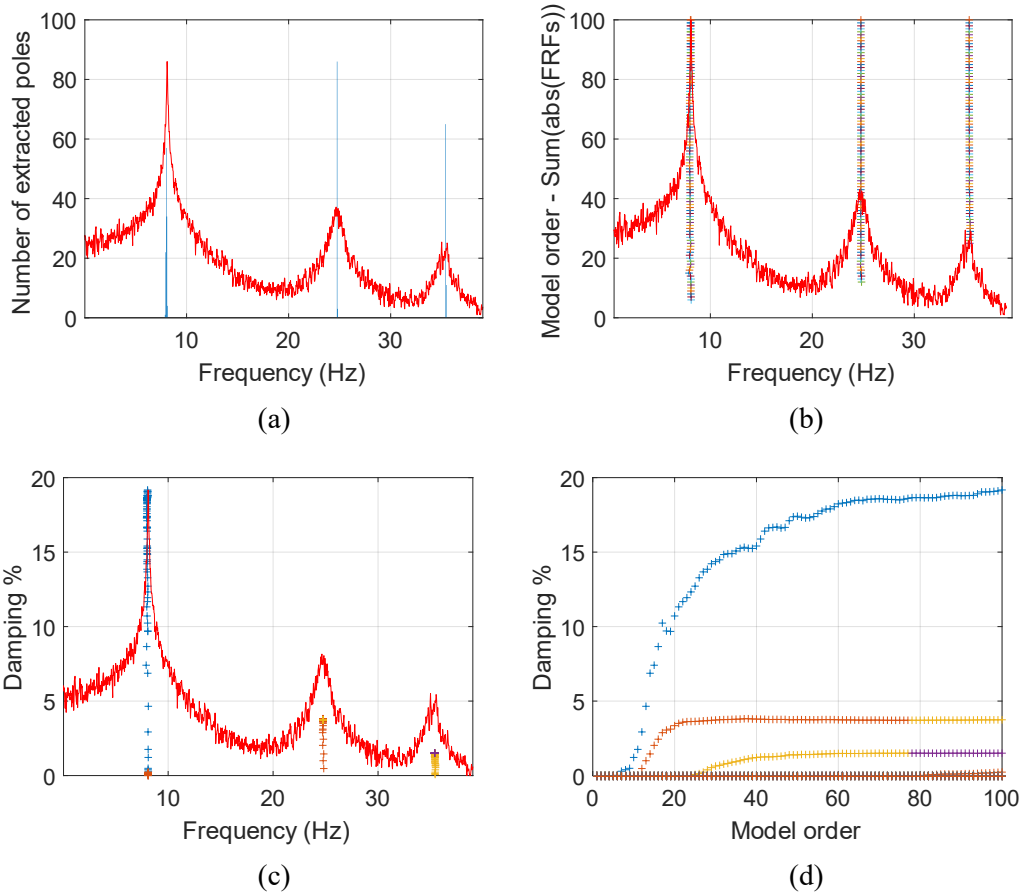




**Fig.3.2.1** ODS FRFs (Mode 7 as reference) obtained from the output time histories with different number of FFT, where (a)  $N_{\text{FFT}} = 2^{12}$ , (b)  $N_{\text{FFT}} = 2^{14}$ , and (c)  $N_{\text{FFT}} = 2^{16}$ .

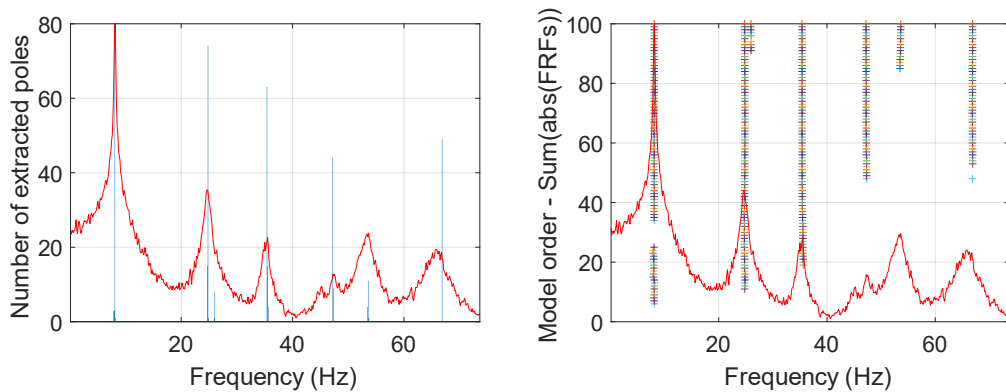
As seen,  $N_{\text{FFT}} = 2^{12}$  and  $2^{14}$  give 6 distinct peaks between 0 and 100Hz, while for  $N_{\text{FFT}} = 2^{16}$  there is too much noise to see 6 distinct peaks between 0 and 100Hz. And, when  $N_{\text{FFT}}$  increases the noise increases. Same as part 3.1, in the following numerical experiments we take  $N_{\text{FFT}}=2^{14}$  and only consider 0-100Hz frequency range for comparison and analysis.

Hereafter, the model order should be determined. This can be done by running the **LIPEZ.m** function with different mode numbers ( $n$ ) within 0-100Hz frequency range. Here in this example, still three different mode numbers, i.e.,  $n = 30, 50$  and  $100$ , are tried and the results can be seen in Fig.3.2.2. And the running times are 37.7s, 100.6s, and 465.2s, which means that the larger the mode number is, the longer time it consumes.



**Fig.3.2.2** (a) Histogram of all the extracted frequencies, overlaid on the sum of the modulus of all the FRFs. (b) The frequencies extracted with an increasing model order overlaid on the sum of the moduli of all the FRFs with a model order being 100. (c) Damping ratios as a function of the frequencies overlaid on the sum of the moduli of all the FRFs with model order being 100. (d) The damping ratios extracted with model order being 100.

In Fig.3.2.2 (a), where the mode number  $n$  reaches 100, the FRFs only get 3 peaks. It is not true, because there are 7 peaks in Fig.3.1.3 (a). It can be caused by the choice of the  $N_{\text{FFT}}$ , which is  $2^{14}$  here. This value is too high, leading to too much noise, hence the last four peaks between 44-46Hz, 47-48Hz, 50-60Hz and 60-70Hz disappear. Therefore, a lower  $N_{\text{FFT}}$  is taken. Specifically, we take  $N_{\text{FFT}}=2^{12}$  with 0-100Hz frequency range, and run the **LIPEZ.m** function again. It takes 37.1s when the mode order is 100, the results can be seen in Fig.3.2.3.



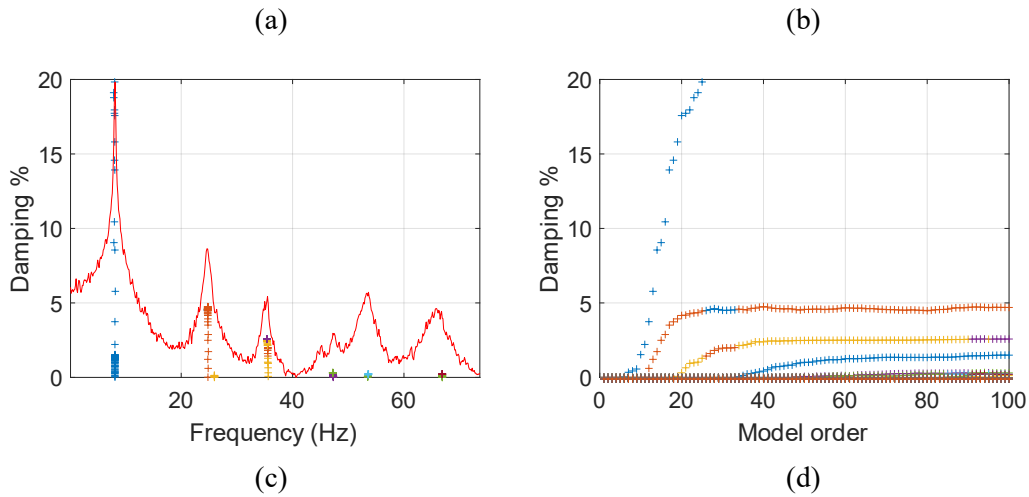


**Fig.3.2.3** (a) Histogram of all the extracted frequencies, overlaid on the sum of the modulus of all the FRFs. (b) The frequencies extracted with an increasing model order overlaid on the sum of the moduli of all the FRFs with a model order being 100. (c) Damping ratios as a function of the frequencies overlaid on the sum of the moduli of all the FRFs with model order being 100. (d) The damping ratios extracted with model order being 100.

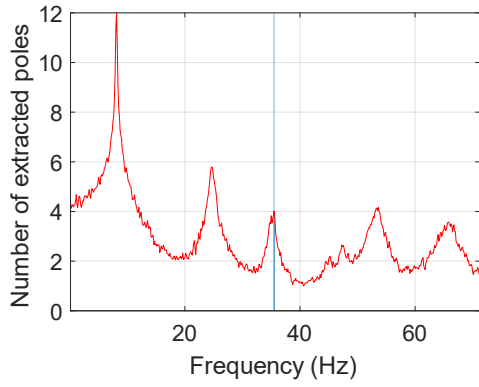
In Fig.3.2.3 (a), where mode number  $n$  reaches 100, it can be seen that the FRFs get 6 peaks this time. There is still one peak missing. However, it behaves better than Fig.3.2.2 (a), where  $N_{\text{FFT}}=2^{14}$ . It means that  $N_{\text{FFT}} = 2^{12}$  is more suitable compared to  $2^{14}$ . Carefully checking the peaks, it can be seen that the missing peak is located within 44-46Hz. And in Fig.3.2.3 (b), the peaks between 47-48Hz, 50-60Hz and 60-70Hz appear as the mode number beyond 50. In the contrast, there is no visible change when the mode number increases in Fig.3.2.2 (a)(b).

But, in order to compare with the previous part 3.1, we still choose  $N_{\text{FFT}} = 2^{14}$  with mode number = 50.

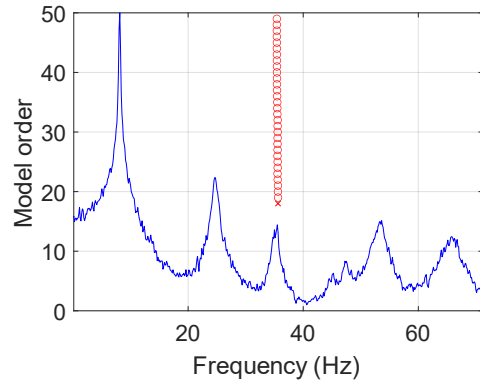
Then, to find the ‘best’ modal parameters, we choose 0-10Hz, 20-30Hz, 30-40Hz, 40-50Hz, 50-60Hz, and 60-70Hz (as Mode 1, Mode 2, Mode 3, Mode 5, Mode 6, and Mode 7) to compare the actual natural frequency, damping ratio and mode shape listed in Table 3.1 and Table 3.2. For reasons of space, we only discuss the ‘good’ case and the ‘worst’ case here, which are Mode 3 and Mode 4, specifically.

Based on the current evidence (Fig.3.2.2 (a)(b) only showing 6 peaks, and some peaks appear with higher mode order than Fig.3.1.2 (b)), it seems that the ODS of Output-Only Method is less accurate than the Input-Output Method.

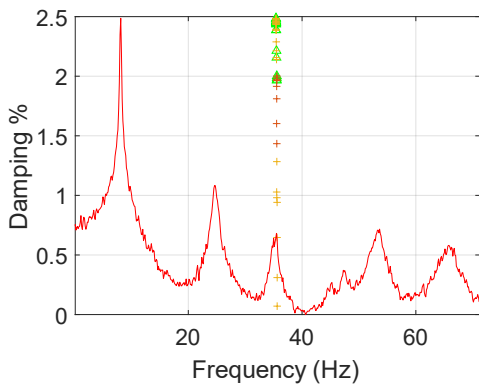
**Mode3: 30-40Hz frequency range with  $N_{\text{FFT}}=2^{14}$ ;  $n=50$ ; 0-100Hz**



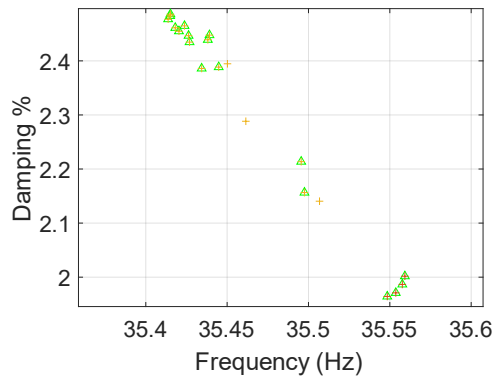
(a)



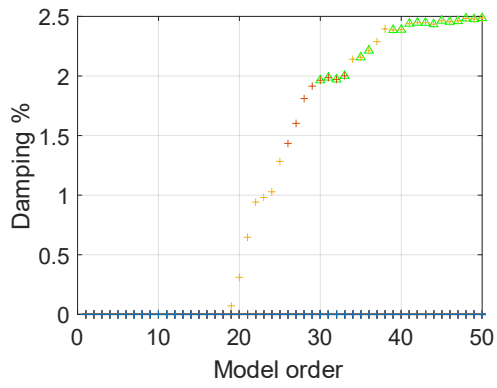
(b)



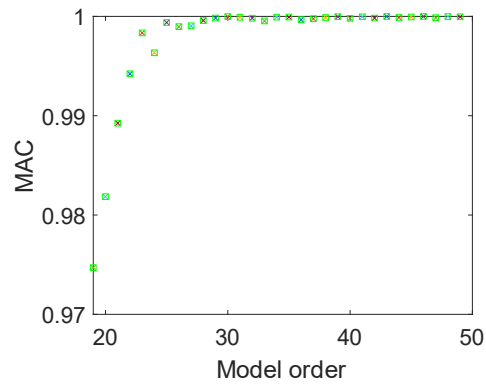
(c)



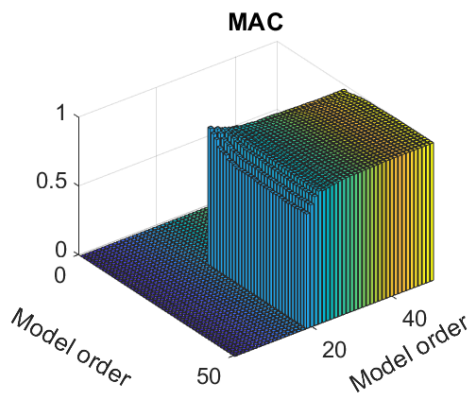
(d)



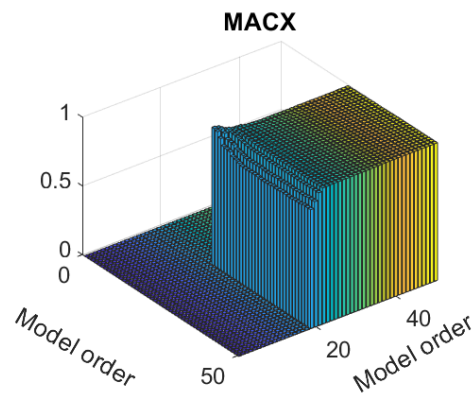
(e)



(f)



(g)



(h)

**Fig.3.2.4** (a) Histogram of all the extracted frequencies, overlaid on the sum of the modulus of all the FRFs. (b) The frequencies extracted with an increasing model order overlaid on the sum of the moduli of all the FRFs with a model order being 100. (c) Damping ratios as a function of the frequencies overlaid on the sum of the moduli of all the FRFs with model order being 100. (d) Local enlargement of (c); (e) The damping ratios extracted with model order being 100. (f) represents the variation of MAC number with respect to the model order. (g) and (h) represent the results of MAC and MACX of this system.

From Fig.3.2.4 (a) it can be seen that the specific natural frequency of Mode 3 is 35.3Hz, close to the actual natural frequency of this system. However, in Fig.3.2.4 (b) the peak appears relatively slowly compared to the input-output case (Fig.3.1.4 (b)). In Fig.3.2.4 (c)(d)(e), the damping ratio does not perform well as there are only a few points are stable. And they are finally stabilized at around 2.45%, which is quite different from the actual damping ratio.

For Fig.3.2.4 (g), it can be seen that all points are close to 1 and belong to stable points. In Fig.3.2.4 (g)(h), it can be seen that most values are close to 1, except for those whose mode order is too small to discover the valid value of MAC and MACX. It means that these mode shapes are similar.

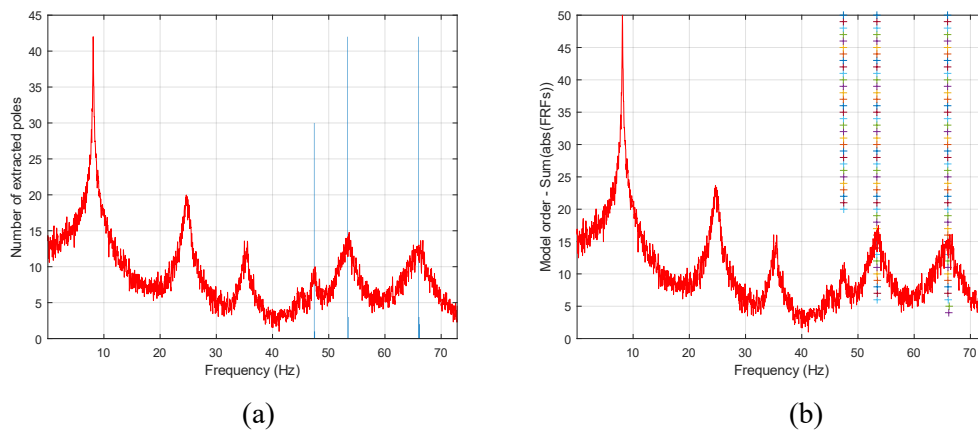
**Table 3.5** Mode shape of 30-40Hz frequency range with  $N_{FFT}=2^{14}$ ,  $n=50$ , and 0-100Hz

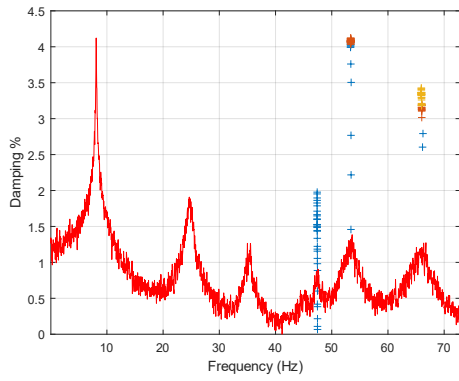
Modal matrix	Mode 1	Mode 2	Mode 3	Mode 4	Mode 5	Mode 6	Mode 7
	3.1616-	5.1204-	1.0000+	-3.3384-	-0.6849-	-3.7975-	1.2434+
	0.5342i	1.0159i	0.0000i	1.5922i	0.1438i	0.4168i	1.2741i

Furthermore, the MAC value based on Table 3.6 and the Mode 3 of Table 3.1 is calculated and the result is 0.8645, close to 1. It suggests that the two mode shapes are similar.

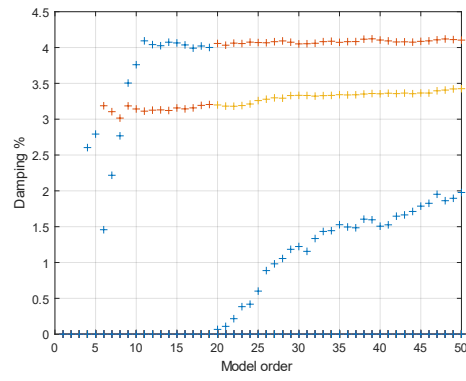
In one word, as far as the evidence is concerned, ODS of output-only method is less accurate than input-output method.

For further analysis of the ODS output-only method, we can narrow the frequency range to 40-80Hz with  $N_{FFT} = 2^{14}$  and mode order = 50, then run the **LIPEZ.m** function again. There is no result. And if we change  $N_{FFT}$  to  $2^{12}$  and narrow the frequency range to 40-80Hz with mode order = 50, the result is attached as below in Fig.3.2.5.





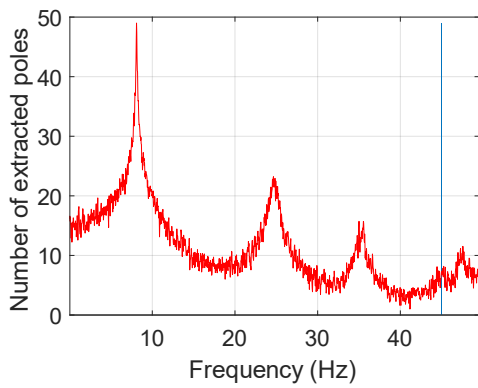
(c)



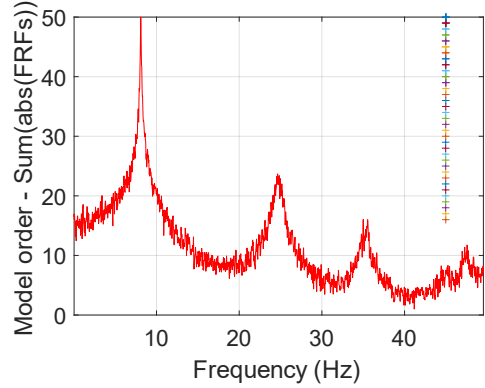
(d)

**Fig.3.2.5** (a)(b)(c)(d) have same meaning with Fig.3.2.2.

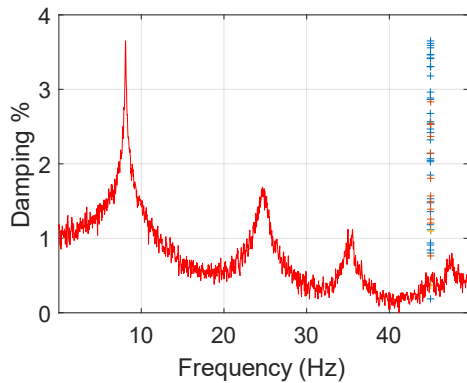
As the Fig.3.2.5 shows, there is still no peaks in 44-46Hz. Then, continue to narrow the frequency range to 44-46Hz, the elapsed time becomes 1.86s and the result is shown in Fig.3.2.6.



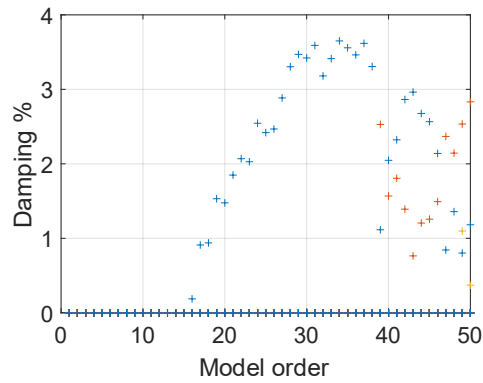
(a)



(b)



(c)

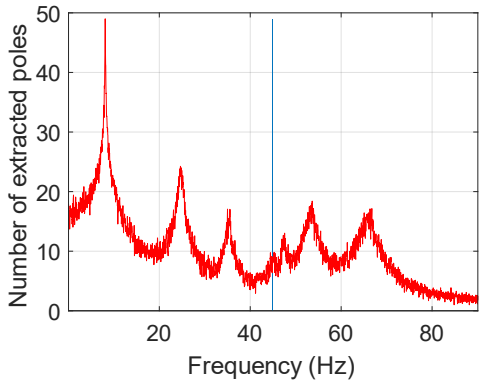


(d)

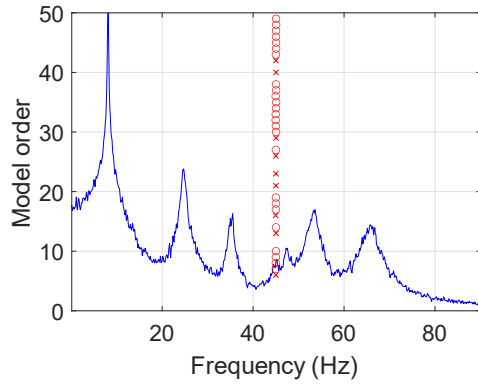
**Fig.3.2.6** (a)(b)(c)(d) have same meaning with Fig.3.2.2.

As the subplots (a) and (b) of Fig.3.2.6 depict, when we narrow the frequency range to 44-46Hz (with  $N_{FFT} = 2^{12}$  and mode order = 50), the peak in 44-46Hz finally appears. Moreover, Fig.3.2.6 (d) does not show stable damping ratio.

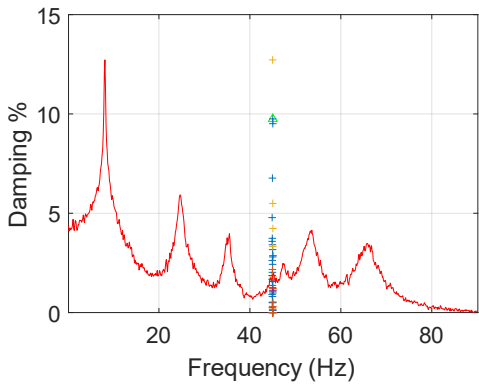
**Mode 4: 44-46Hz frequency range with  $N_{FFT}=2^{12}$ ,  $n=50$ , and 44-46Hz**



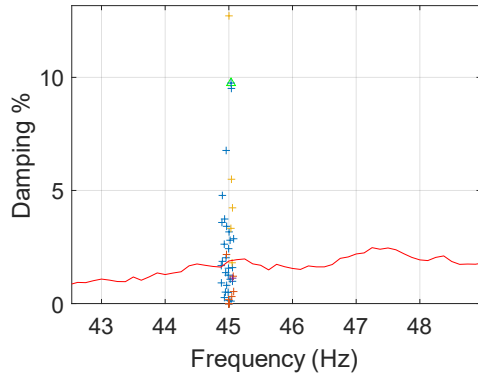
(a)



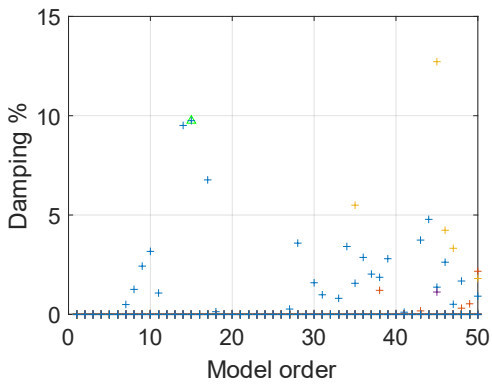
(b)



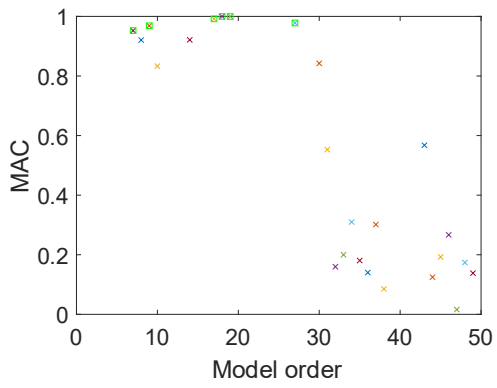
(c)



(d)

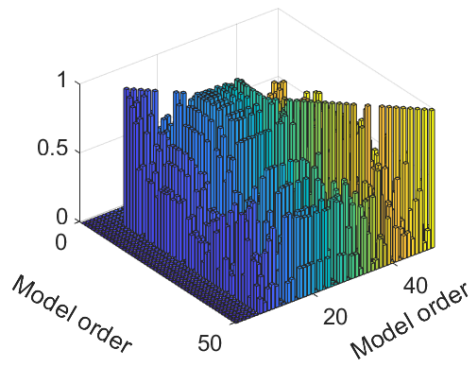


(e)



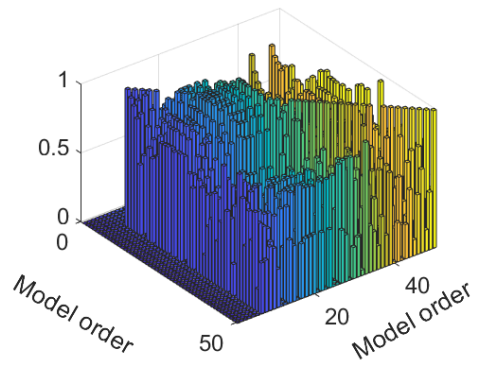
(f)

**MAC**



(g)

**MACX**



(h)

**Fig.3.2.7** (a)(b)(c)(e) have same meaning with Fig.3.2.2 in addition to including stabilized images. (d) enlarge of (c); (f) represent MAC number; (g)(h) represent MAC and MACX of this system.

From Fig.3.2.7 (a), it can be seen that the specific natural frequency of Mode 4 is 45Hz. In Fig.3.2.7 (b) the peak does not appear sufficiently quickly and there are many unstable points. For Fig.3.2.7 (c)(d)(e), it is difficult to read the stable damping ratio.

In Fig.3.2.7 (f), only few points are stable and close to 1, which means that, for mode 4, most of the mode shapes are dissimilar as the mode number varies. For Fig.3.2.7 (g)(h), it can be seen that, for Mode 4, varying n gives quite different results of mode shapes.

**Table 3.7** Mode shape of 44-46Hz frequency range with  $N_{FFT}=2^{12}$ , and  $n=50$

<b>Modal matrix</b>	<b>Mode 1</b>	<b>Mode 2</b>	<b>Mode 3</b>	<b>Mode 4</b>	<b>Mode 5</b>	<b>Mode 6</b>	<b>Mode 7</b>
	0.0811-	-1.3743-	1.0000	-0.2785	0.2535-	-0.1934-	-0.0334
	0.2077i	0.0113i	+0.0000i	+1.8824i	0.5612i	1.5631i	+0.7577i

Furthermore, we can compute the MAC value using data provided by the Table 3.7 and Mode 4 in Table 3.1, whose result is 0.6946. It means that they are quite different.

In summary, compared with the ODS of the output-only method, the input-output method has higher accuracy in terms of the natural frequency, damping ratio, mode shape, etc., whose good results are hard to obtain with the output-only condition.



### 3.2.2 CPSD (Cross Power Spectral Density)

This section describes the numerical results of LIPEZ when cross power spectral density (CPSD) function is used instead of ODS-FRF. Same with ODS method, in this case still choose point 7 as the reference. To obtain the CPSD FRF only based on the output time histories by using equation (3.5).

Then, still change the  $N_{\text{FFT}}$  and plot the obtained CPSD FRF. The results are attached in Fig.3.2.8, where (a), (b), and (c) indicate  $N_{\text{FFT}} = 2^{12}$ ,  $2^{14}$ , and  $2^{16}$  respectively.

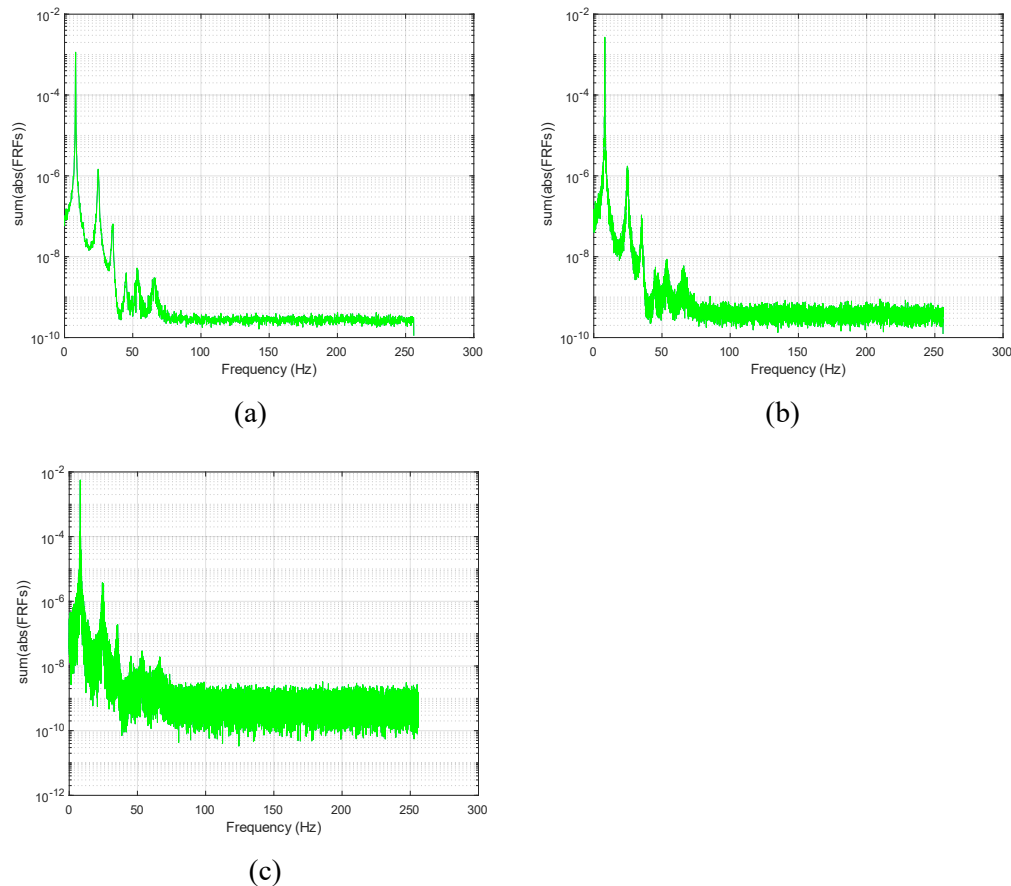


**Fig.3.2.8** CPSD FRF (Mode 7 as reference) obtained from Fast Fourier Transform (FFT) onto only the output time histories with different number of FFT, where (a)  $N_{\text{FFT}} = 2^{12}$ , (b)  $N_{\text{FFT}} = 2^{14}$ , and (c)  $N_{\text{FFT}} = 2^{16}$ .

As seen,  $N_{\text{FFT}} = 2^{12}$  and  $2^{14}$  give 6 distinct peaks between 0 and 100Hz, while for  $N_{\text{FFT}} = 2^{16}$  there is too much noise to see 6 distinct peaks between 0 and 100Hz. And, when  $N_{\text{FFT}}$  increases the noise increases. Same as part 3.1, in the following numerical experiments we take  $N_{\text{FFT}}=2^{14}$  and only consider 0-100Hz frequency range for comparison and analysis.

Hereafter, the model order should be determined. This can be done by running the **LIPEZ.m** function with different mode numbers ( $n$ ) within 0-100Hz. For this example, still three different mode numbers, i.e.,  $n = 30, 50$  and  $100$ , are tried and the results can be seen in Fig.3.2.9. The running times are 38.0s, 107.7s and 529.2s. This means that the larger the mode number, the more time it takes.

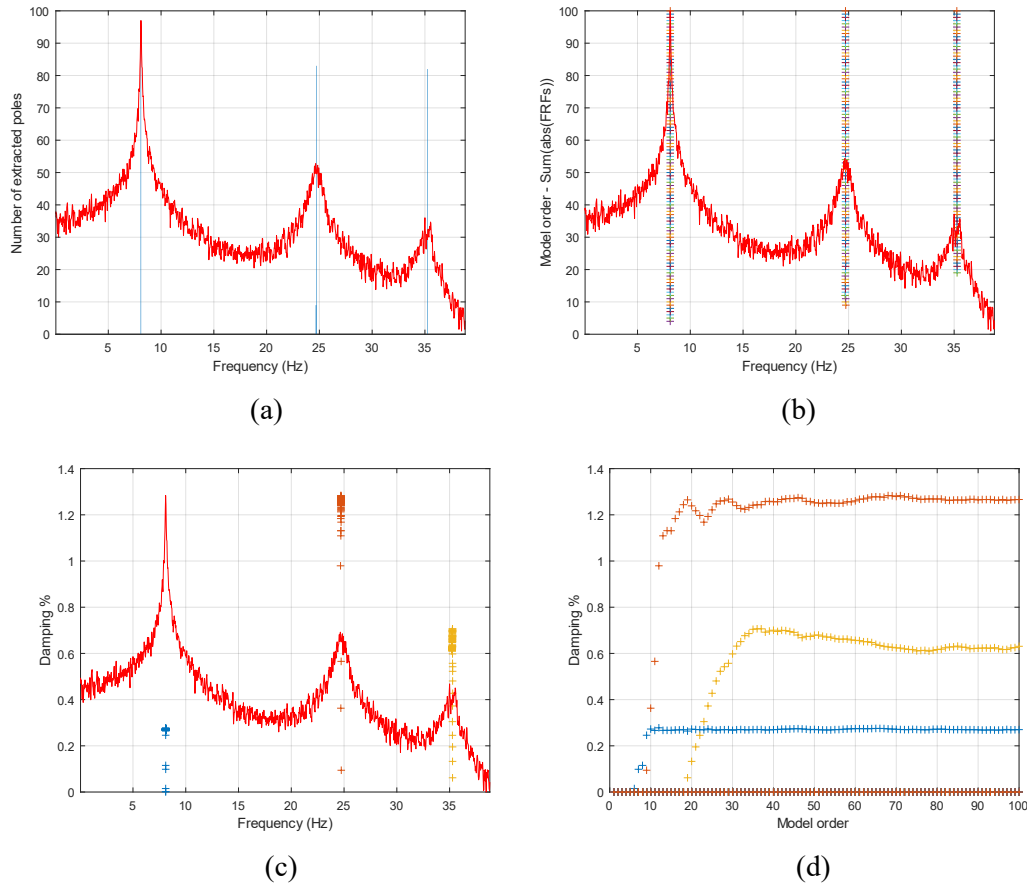
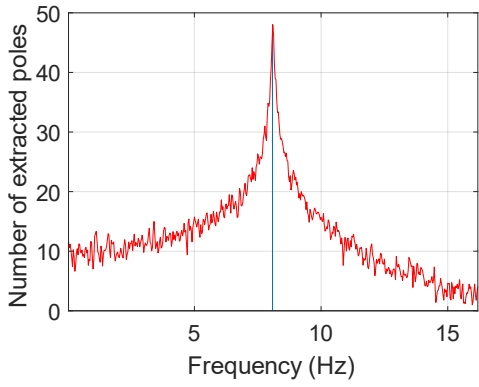


**Fig.3.2.9** (a) Histogram of all the extracted frequencies, overlaid on the sum of the modulus of all the FRFs. (b) The frequencies extracted with an increasing model order overlaid on the sum of the moduli of all the FRFs with a model order is 100. (c) Damping ratios as a function of the frequencies overlaid on the sum of the moduli of all the FRFs with model order is 100. (d) The damping ratios extracted with model order is 100.

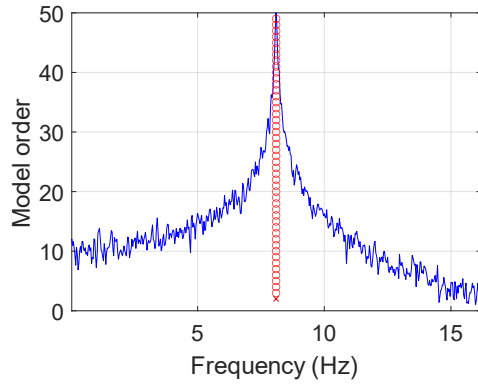
It can be seen in Fig.3.2.9 (a), there only detected 3 peaks of FRF (that's not true, because we can get 7 peaks at Fig.3.1.2). Furthermore, as can be seen in Fig.3.2.9 (d), when the mode number increases, the damping ratios approach corresponding constant values. In this way, same as before  $n$  is equal to 100 certainly gives the best result. However, it has also the highest time consumption among the three. Therefore, considering the balance between the result and time expense, mode order is equal to 50 seems to be a better choice.

Like before, to find the 'best' modal parameters we set 0-10Hz, 20-30Hz, 30-40Hz (as Mode 1, Mode 2, Mode 3) to compare the actual natural frequency, damping ratio and modal matrix in Table 3.1 and Table 3.2. For reasons of space, we only discuss Mode1, Mode 3, and Mode 4 ( $N_{FFT}=2^{12}$ ; mode order is 50; 40-80Hz).

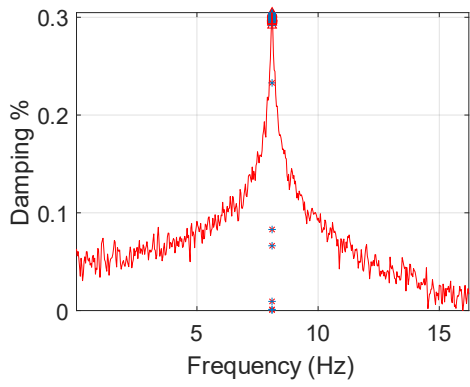
**Mode 1: 0-10Hz frequency range with  $N_{FFT}=2^{14}$ ;  $n=50$ ; 0-100Hz**



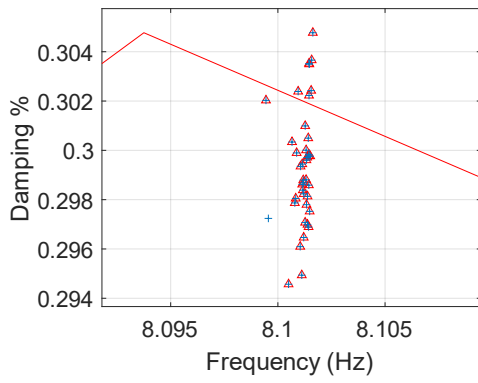
(a)



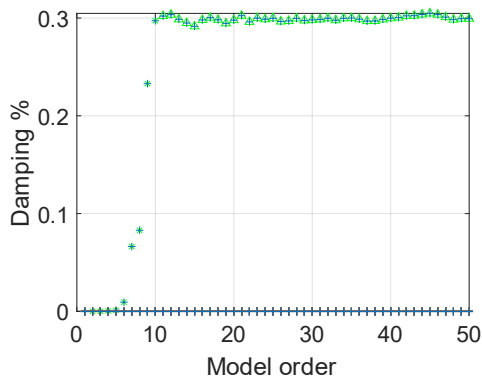
(b)



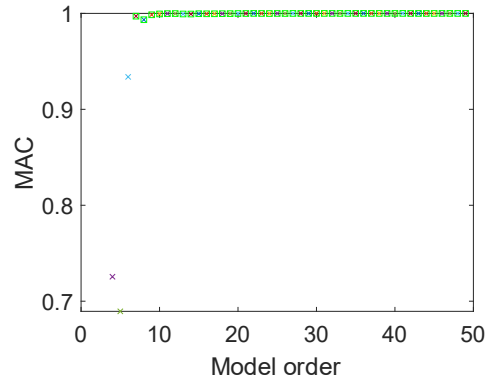
(c)



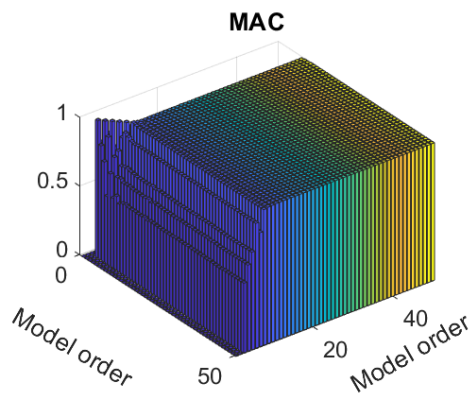
(d)



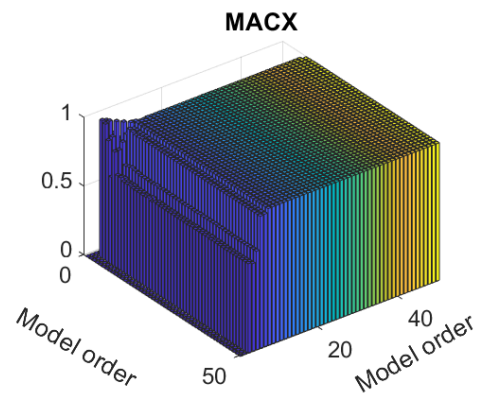
(e)



(f)



(g)



(h)

**Fig.3.2.10** (a)(b)(c)(e) have same meaning with Fig.3.2.2 in addition to including stabilized images.(d) is the zoom of (c). (g) and (h) represent MAC and MACX of this system.

From Fig.3.2.10 (a), the specific natural frequency of mode 1 is 8.1Hz. In Fig.3.2.10 (b) the peak appears quick and only the first node is unstable. In Fig.3.2.10 (c)(d), the damping ratio is located around 0.3%. The same conclusion we can get from Fig.3.2.10 (e). And compare to natural frequency and damping ratio in Table 3.1 Mode 1. We will find that the error is 0.12% and 36.4%.

For Fig.3.2.10 (f), it can be seen that when the mode order is small, the mode shape of Mode 1 is unstable. But when the mode order increases, the mode shape of Mode 1 is stable and similar because their MAC number is highly close to 1.

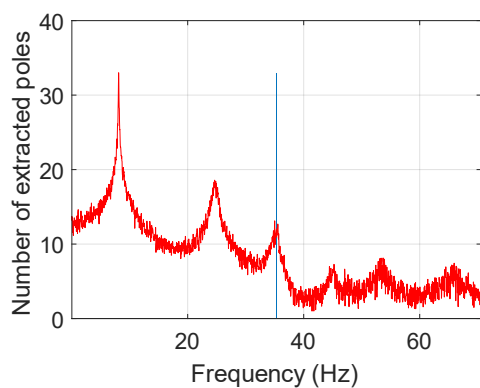
In Fig.3.2.10 (g)(h) same as before, we only discuss the valid part. When the mode order is small, the mode shapes of Mode 1 are not similar enough. But the similarity will be increased as the mode order is increase, once the mode order is large enough, the mode shapes of Mode 1 are highly similar because the MAC and MACX number is close to 1.

**Table 3.8** Modal shape of 0-10Hz frequency range with  $N_{FFT}=2^{14}$ ;  $n=50$ ; 0-100Hz

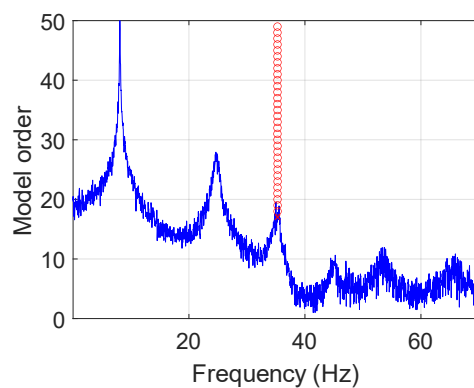
	Mode 1	Mode 2	Mode 3	Mode 4	Mode 5	Mode 6	Mode 7
<b>Modal matrix</b>	0.5215 +0.0115i	0.9985+ 0.0316i	1.0000 + 0.0000i	1.1576- 0.0078i	1.1361+ 0.0645i	1.2427 +0.0271i	1.3687- 0.0008i

Compute MAC number by using Table 3.8 and Table 3.1 Mode 1 to get MAC is equal to 0.9995, close to 1, which mean two mode shapes are extremely similar.

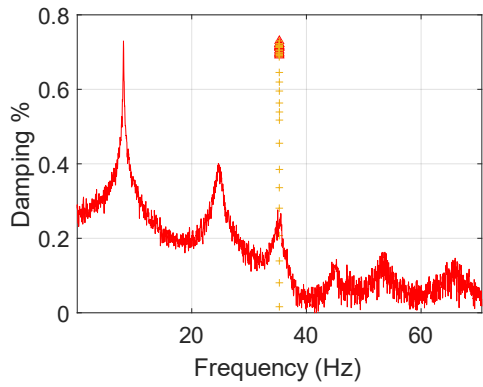
**Mode 3: 30-40Hz frequency range with  $N_{FFT}=2^{14}$ ;  $n=50$ ; 0-100Hz**



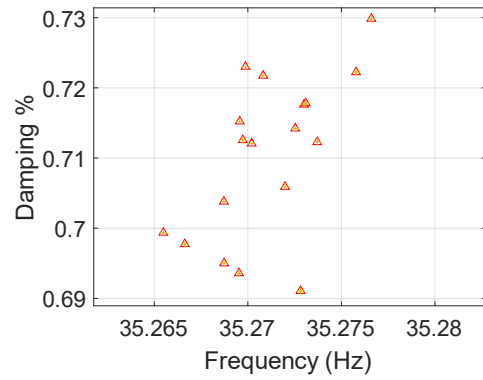
(a)



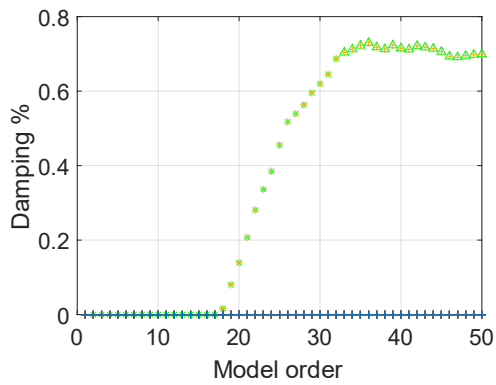
(b)



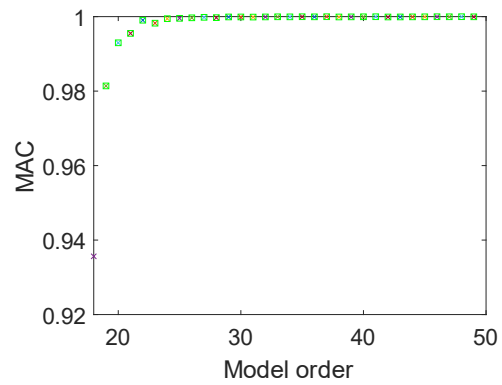
(c)



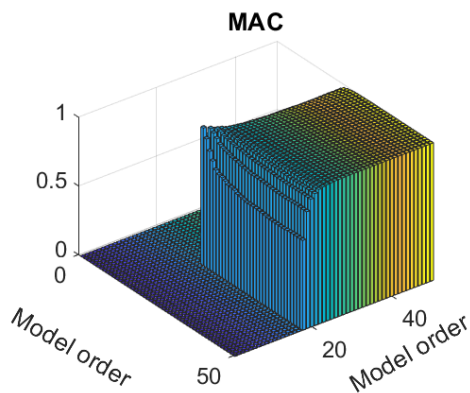
(d)



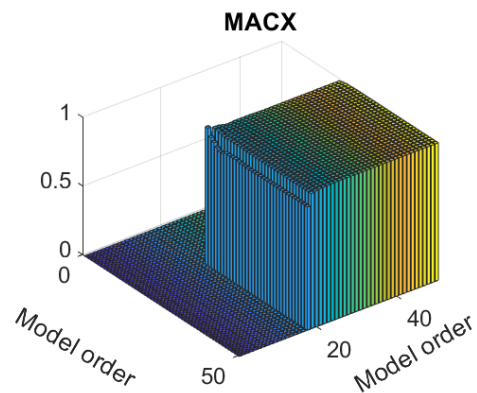
(e)



(f)



(g)



(h)

**Fig.3.2.11** (a)(b)(c)(e) have same meaning with Fig.3.2.2 in addition to including stabilized images.(d) is the zoom of (c). (g) and (h) represent MAC and MACX of this system.

From Fig.3.2.11 (a), the specific natural frequency of Mode 3 is 35.3Hz. For Fig.3.2.11 (c)(d)(e), the stable damping ratio is 0.71%. The error between the actual data is close to 0.06% and 51%.

In Fig.3.2.11 (e), all nodes are stable and close to 1, which means most mode shapes of Mode 3 with different mode number are similar. For Fig.3.1.11 (g)(h), it can be seen that the most mode shape of Mode 3 are similar.

**Table 3.9** Modal shape of 30-40Hz frequency range with  $N_{FFT}=2^{14}$ ;  $n=50$ ; 0-100Hz

Modal matrix	Mode 1	Mode 2	Mode 3	Mode 4	Mode 5	Mode 6	Mode 7
	2.3030-	3.1144-	1.0000 +	-2.7940	-0.1705 +	-3.0293 +	2.2632
	0.1513i	0.4280i	0.0000i	+0.046i	0.0161i	0.2104i	+0.061i

Compute MAC use Table 3.9 and Table 3.1 Mode 3 get MAC is 0.992, which mean two mode shapes are highly similar.

Then, narrow the frequency band to 40-80Hz and running the **LIPEZ.m** function again. But that's impossible, there is no result at all. For further analysis of the CPSD output-only method, we can narrow the frequency range to 40-80Hz with  $N_{FFT} = 2^{12}$  and mode order = 50, then run the **LIPEZ.m** function again.

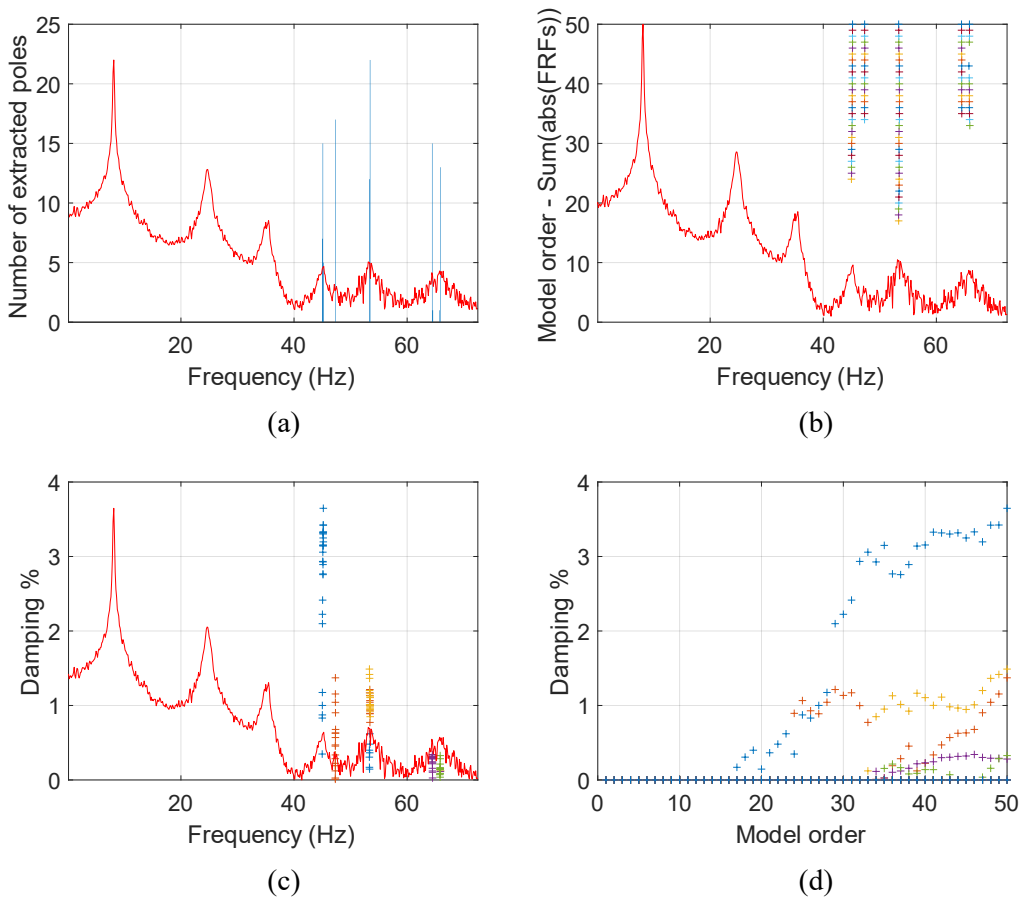
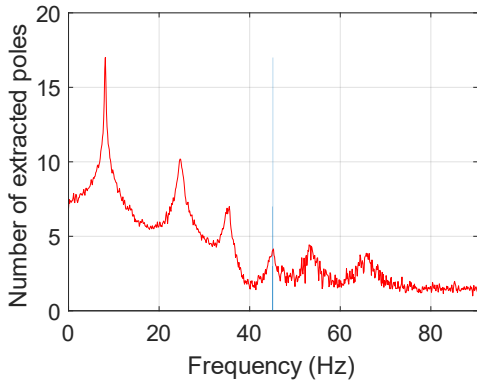


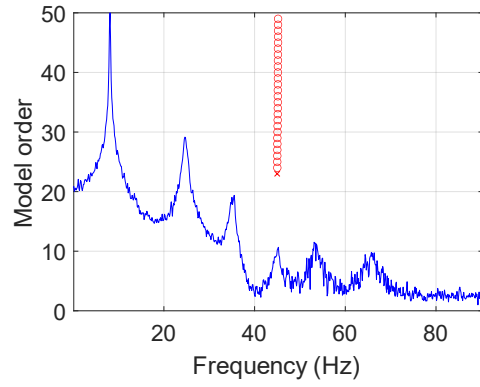
**Fig.3.2.12** (a) Histogram of all the extracted frequencies, overlaid on the sum of the modulus of all the FRFs. (b) The frequencies extracted with an increasing model order overlaid on the sum of the moduli of all the FRFs with a model order is 50. (c) Damping ratios as a function of the frequencies overlaid on the sum of the moduli of all the FRFs with model order is 50. (d) The damping ratios extracted with model order is 50.

As the subplots (a) and (b) of Fig.3.2.12 shows, when we narrow the frequency range to 40-80Hz (with  $N_{FFT}$  is  $2^{12}$  and mode order is 50), the last four peaks appear.

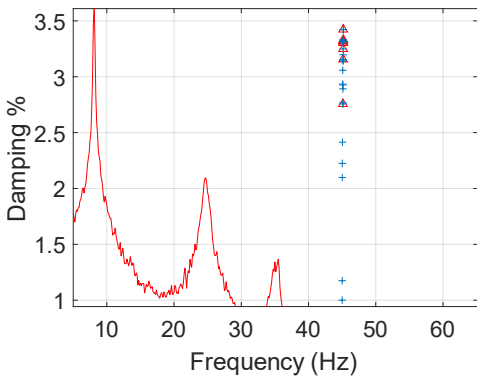
**Mode 4: 44-46Hz frequency range with  $N_{FFT}=2^{12}$ ;  $n=50$ ; 40-80Hz**



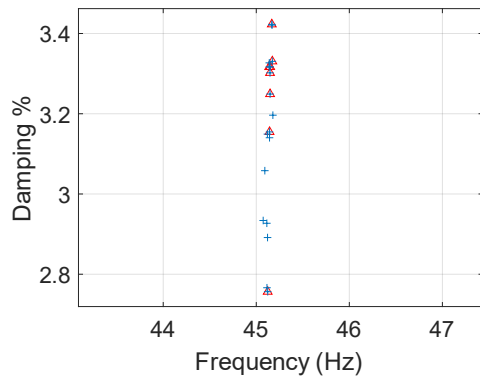
(a)



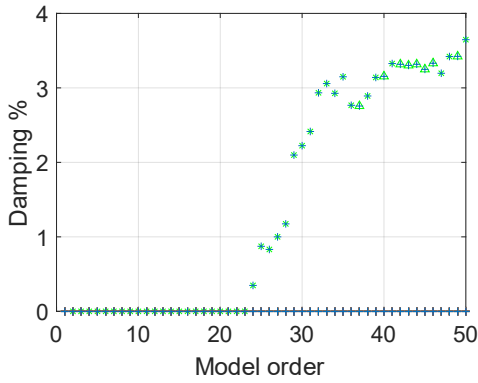
(b)



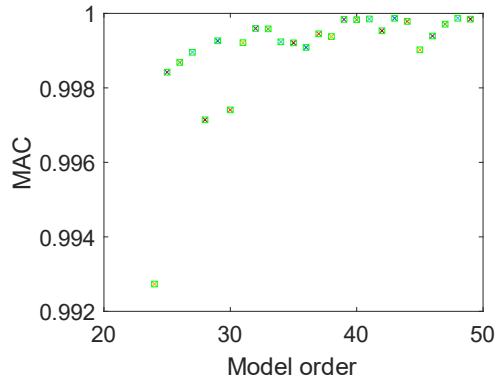
(c)



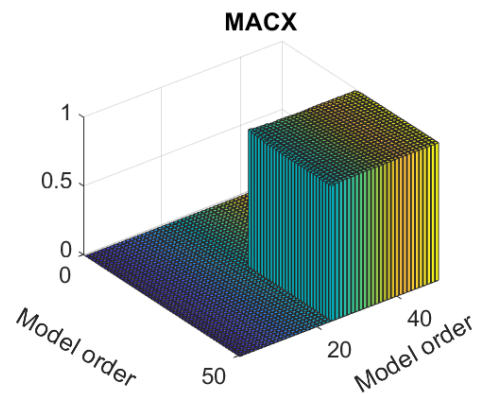
(d)



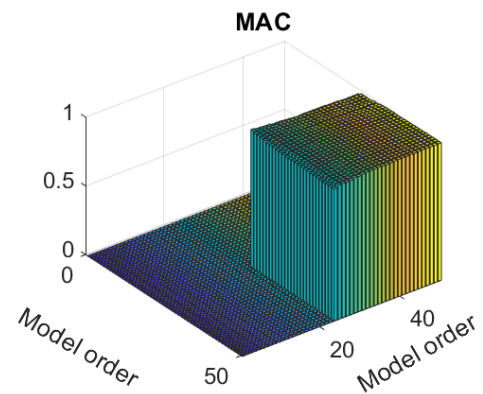
(e)



(f)



(g)



(h)

**Fig.3.2.13** (a)(b)(c)(e) have same meaning with Fig.3.2.2 in addition to including stabilized images. (d) enlarge of (c); (f) represent MAC number; (g)(h) represent MAC and MACX of this system.

From Fig.3.2.13 (a) it can be seen that the specific natural frequency of Mode 4 is 45.1Hz, close to the natural frequency of Mode 1 in Table 3.1. Except for the first point in Fig.3.2.13 (b), the others are stable points. For Fig.3.2.13 (c)(d)(e), It can be seen that the damping ratio of the Mode 4 is located around 3.3%, quite different with actual damping ratio of Mode 4.

In Fig.3.2.13 (f), most points are stable and close to 1, which means most mode shapes of Mode 4 with different mode number are similar. For Fig.3.2.13 (g)(h), it can be seen that, for Mode 4, varying n gives similar results of mode shapes.

**Table 3.10** Mode shape of 44-46Hz frequency range with  $N_{FFT}=2^{12}$ ;  $n=50$ ; 40-80Hz

Mode shape	Mode 1	Mode 2	Mode 3	Mode 4	Mode 5	Mode 6	Mode 7
	-0.2890 - 2.4532i	-1.8171 + 0.0615i	1.0000+ 0.0000i	1.4323 + 5.9240i	-0.8820 - 1.7624i	-1.2395 - 5.0313i	0.3073 + 1.7574i

Furthermore, the MAC value based on Table 3.10 and the Mode 3 of Table 3.1 is calculated and the result is 0.9253, close to 1. It suggests that the two mode shapes are similar.

Obviously, the ODS of Output-Only Method has lower operability and accuracy than the of CPSD Output-Only Method. To conclude, as can be seen from the above part. Whether it is the stability seen from the image or the accuracy compared from the calculated data or operability, the Input-Output Method have best performance, the CPSD of Output-Only Method second, and the ODS of Output only method is the worst.



### 3.3 Automated selection algorithm

In this section, we use the automated selection algorithm to select the ‘best’ modal parameters to deal with the data operated by LIPEZ in 3 cases, respectively input-output case, ODS-FRF output-only case, and CPSD output-only case.

The automated selection algorithm is a fully automatic method of selecting the best modal parameter without requiring user participation (including setting thresholds, changing parameters, etc.) when estimating modal parameters. It mainly consists of three steps.

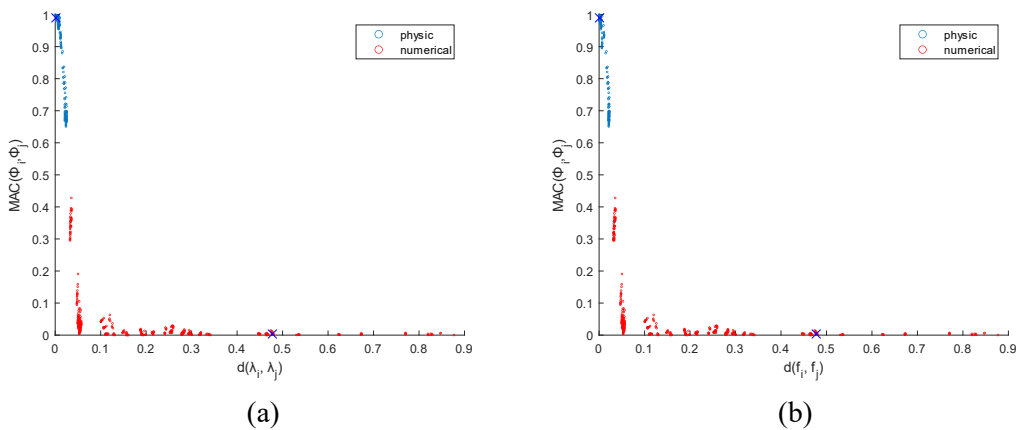
The first step is to select as much data as possible and use soft and hard criteria to remove the spurious modes. During this step, numerous modes are divided into two groups, i.e., ‘physic’ and ‘numerical’. The former means possibly physical modes, while the latter refers certainly spurious ones, which will be removed, hence a preliminary cleared stabilization diagram is obtained. The detailed soft and hard criteria used can be found in [3].

As for the second step, it is to group those similar modes obtained from the previous step, realized through a hierarchical clustering approach. This step yields a set of mode groups with corresponding number of elements, according to their degree of similarity quantitized by the so-called mutual distances. Based on the groups obtained from the second step, the third step is able to select all the certainly physical modes and remove all the remaining spurious ones. It is realized through a 2-mean algorithm that is fully explained in [3]. Finally, the best modal parameters can be obtained by drawing the latest stabilization diagram.

As all the above procedures can be automatically operated without needing manual interaction, according to the literature, this method realizes a fully automated modal analysis procedure. Further details on this algorithm can be found in [3].

#### 3.3.1 Input-output case

Run the script `ASA.m` in MATLAB, using the data obtained from the LIPEZ method input-output case. It can be seen that the operation time is 6.83s, and the result can be seen at Fig.3.3.1, Table 3.11, and Table 3.12.



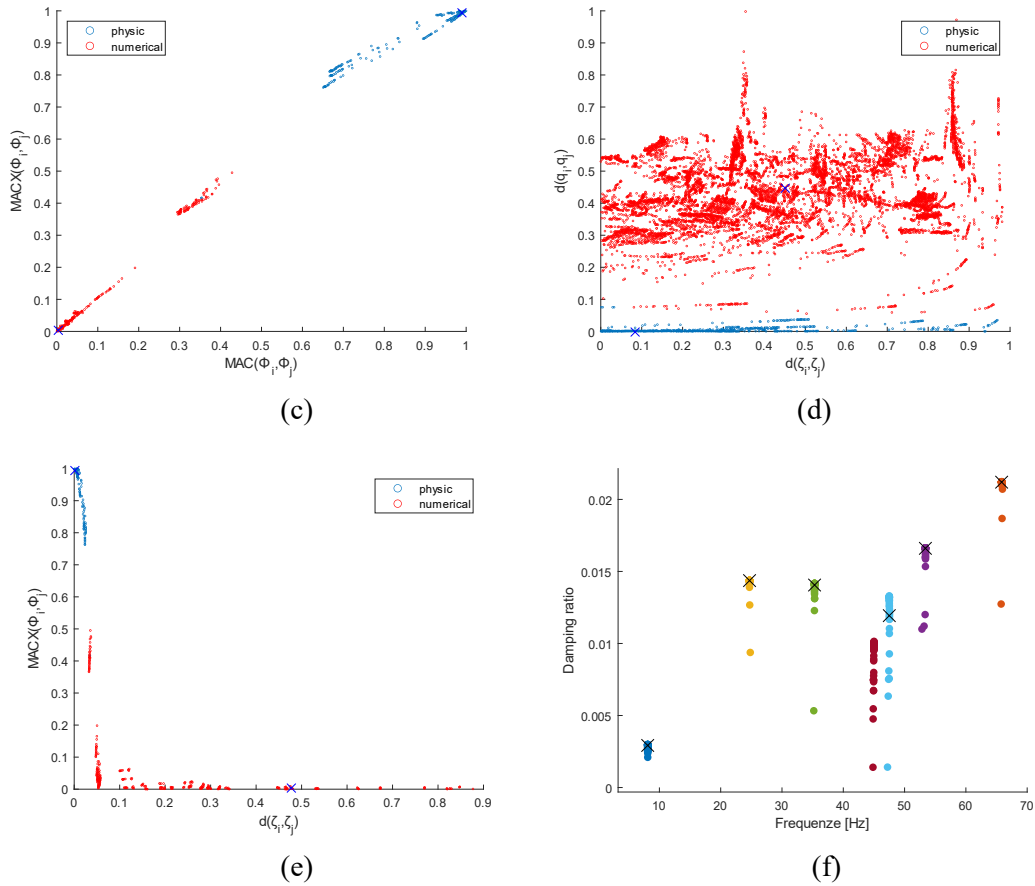


**Fig.3.3.1** the possibly physical modes (blue circle) and certainly spurious modes (red circle), obtained after applying the stabilization (a) eigenvalue distance vs. MAC; (b) frequency distance vs. MAC; (c) MAC vs. MACX; (d) damping ratio distance vs. the modal scaling factors distance; (e) damping ratio distance vs. MACX (the blue cross: final centroids). (f) represent the damping ratio vs. natural frequency diagram of all modes in the physical mode sets (dots), and their representatives (black crosses).

Fig.3.3.1 (a)(b)(c)(d)(e) show all the points performed after Step 1. For example, (a) eigenvalue distance vs. MAC, which first represents the soft criterion VS1[3] and VS4[3]. When VS1 is equal to 0, that mode belongs to the ideal physical mode; when VS1 is equal to 1, that mode belongs to the ideal spurious mode. If VS1 of this mode is closer to 0, this mode belongs to ‘physic’, vis versa, this mode belongs to ‘numerical’. The same process for VS4. After, using hard criterion VH1, VH2, and VH3[3] eliminate ineligible modes. Blue cross represent the final centroids of ‘physic’ and ‘numerical’ group.

Fig.3.3.1(f) is the final result of the natural frequency and damping ratio, in which we are more interested. The black cross in Fig.3.3.1(f) is the average of their set, which can better indicate the ‘best’ modal parameter located.

**Table 3.11 Through automated selection algorithm, the final natural frequency and damping ratio from Fig.3.3.1 (f)**

	Mode 1	Mode 2	Mode 3	Mode 4	Mode 5	Mode 6	Mode 7
<b>Natural frequency (Hz)</b>	8.1	24.7	35.3	45.0	47.5	53.4	65.8
<b>Damping ratio (%)</b>	0.29	1.43	1.41	No value	1.2	1.66	2.11
<b>Error<sub>NF</sub> (%)</b>	0.12	0.00	0.06	0.07	0.11	0.11	0.29
<b>Error<sub>DR</sub> (%)</b>	31.82	0.69	1.40	No value	13.04	3.11	7.11

The third and fourth rows of Table 3.11 is the error between the final natural frequency and damping ratio through the automated selection algorithm and the ideal modal parameters in Table 3.1. It can be seen that the final natural frequency are highly similar to the ideal data. But not for the damping ratio, the error is quite large. Even more, there is no result of the damping ratio in Mode 4.

**Table 3.12 The ‘best’ mode shape through automated selection algorithm**

Mode 1	Mode 2	Mode 3	Mode 4	Mode 5	Mode 6	Mode 7
0.5127- 0.0108i	0.8066 - 0.0133i	2.4298 - 0.1526i	No value	7.5377 - 3.8397i	-0.4707 - 0.0081i	-0.2676 - 0.0063i
0.9824- 0.0234i	1.3429 - 0.0132i	3.3105 - 0.0988i		-4.0672 + 2.3463i	-0.6885 + 0.0012i	-0.1029 + 0.0041i
1.0000+ 0.0000i	1.0000 + 0.0000i	1.0000 + 0.0000i		1.0000 + 0.0000i	1.0000 + 0.0000i	1.0000 + 0.0000i
1.1609 - 0.0265i	0.7555 - 0.0223i	-2.7155 + 0.0146i		0.5393 - 0.5180i	-0.4517 - 0.0120i	-0.1117 - 0.0102i
1.1428 - 0.0266i	0.4269 + 0.0185i	-0.4913 + 0.0187i		-0.4941 + 0.2827i	1.4082 + 0.0300i	-0.8329 + 0.0383i
1.2499 - 0.0243i	-0.3745 + 0.0167i	-3.2772 + 0.2491i		0.0005 + 0.0574i	-0.5319 - 0.0118i	0.2179 - 0.0111i
1.3581 - 0.0208i	-3.0035 + 0.0289i	2.4578 - 0.1304i		0.1897 - 0.0094i	-0.0281 + 0.0229i	0.0227 - 0.0107i
MAC						
0.9999	0.9998	0.9982	No value	0.9881	0.9986	0.9975

The last row of Table 3.12 is the mac number of the final mode shape of each mode compared to the ideal data. And they are all close to 1 (except mode 4).

In conclusion, the accuracy of automated selection algorithm for mode shape in this case is fairly good.

### 3.3.2 ODS-output only case

Run the script **ASA.m** in MATLAB, using the data obtained from the LIPEZ method ODS output-only case (case 1:  $N_{FFT} = 2^{14}$ , mode order = 50, frequency range = 0-100Hz for first three modes; case 2:  $N_{FFT} = 2^{12}$ , mode order = 50, frequency range = 40-80Hz last three modes). It can be seen that the operation time are 2.45s and 2.73s, and the result can be seen at Fig.3.3.2, Table 3.13, and Table 3.14 for case1 and Fig.3.3.3, Table 3.15, and Table 3.16 for case 2.

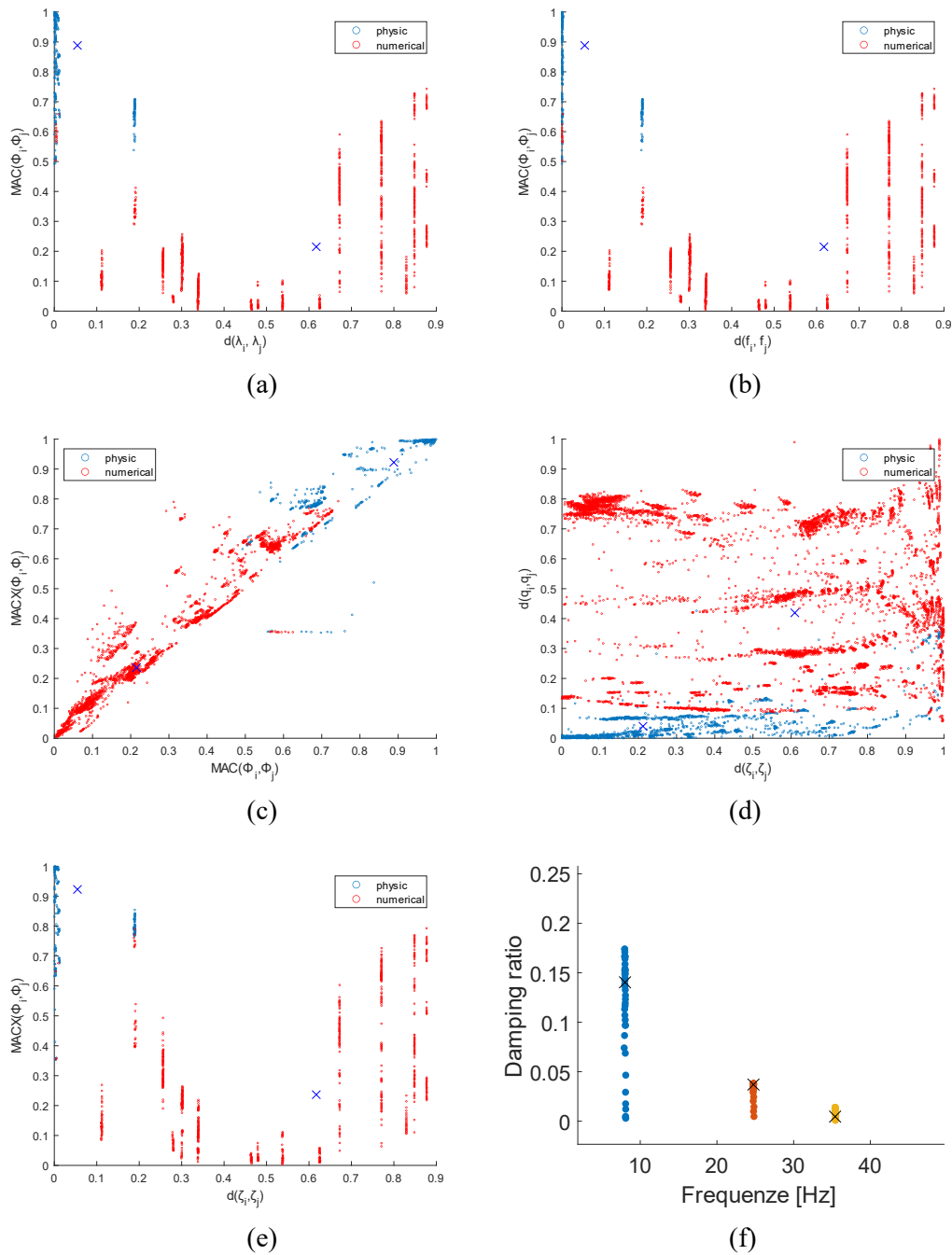


**Fig.3.3.2** The possibly physical modes (blue circle) and certainly spurious modes (red circle), obtained after applying the stabilization (a) eigenvalue distance vs. MAC; (b) frequency distance vs. MAC; (c) MAC vs. MACX; (d) damping ratio distance vs. the modal scaling factors distance; (e) damping ratio distance vs. MACX (the blue cross: final centroids). (f) represent the damping ratio vs. natural frequency diagram of all modes in the physical mode sets (dots), and their representatives (black crosses).

**Table3.13** Through automated selection algorithm, the final natural frequency and

**damping ratio from Fig.3.3.2 (f)**

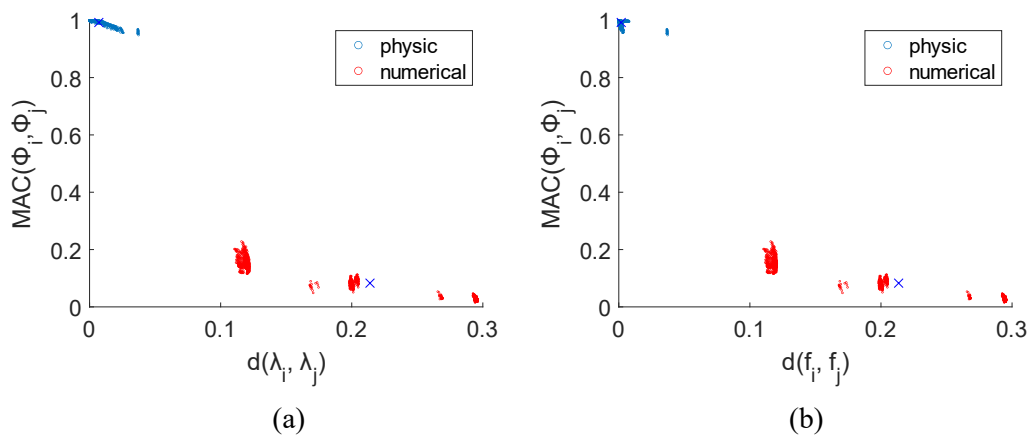
	<b>Mode 1</b>	<b>Mode 2</b>	<b>Mode 3</b>
<b>Natural frequency (Hz)</b>	8.01	24.8	35.4
<b>Damping ratio (%)</b>	0.1403	0.037	0.0046
<b>Error<sub>NF</sub> (%)</b>	0.12	0.00	0.06
<b>Error<sub>DR</sub> (%)</b>	36.23	97.43	99.68

From Table 3.13, it can be seen that the final natural frequency is highly similar to the ideal data. But not for the damping ratio, the error is quite large.

**Table3.14 The final mode shape through automated selection algorithm**

<b>Mode 1</b>	<b>Mode 2</b>	<b>Mode 3</b>
0.5116 - 0.0223i	0.7801- 0.0691i	2.3690- 0.9806i
1.0030 - 0.1117i	1.2188 - 0.2257i	3.6116 - 2.0047i
1.0000 - 0.0000i	1.0000 + 0.0000i	1.0000 + 0.0000i
1.1679 - 0.1787i	0.6909 - 0.5074i	-4.0867 - 1.3467i
1.1496 - 0.1720i	0.3952 - 0.3637i	-1.0250 - 0.0563i
1.2768 - 0.3204i	-0.3880 - 0.5220i	-3.8279+ 0.1366i
1.1958 - 0.3460i	-2.4074 - 0.1619i	2.0197 + 2.0784i
<b>MAC</b>		
0.9898	0.9237	0.8074

The last row of Table 3.14 is the MAC number of the final mode shape of each mode compare the ideal data. There are close to 1, which means that the accuracy of automated selection algorithm for mode shape in this case is fairly good.



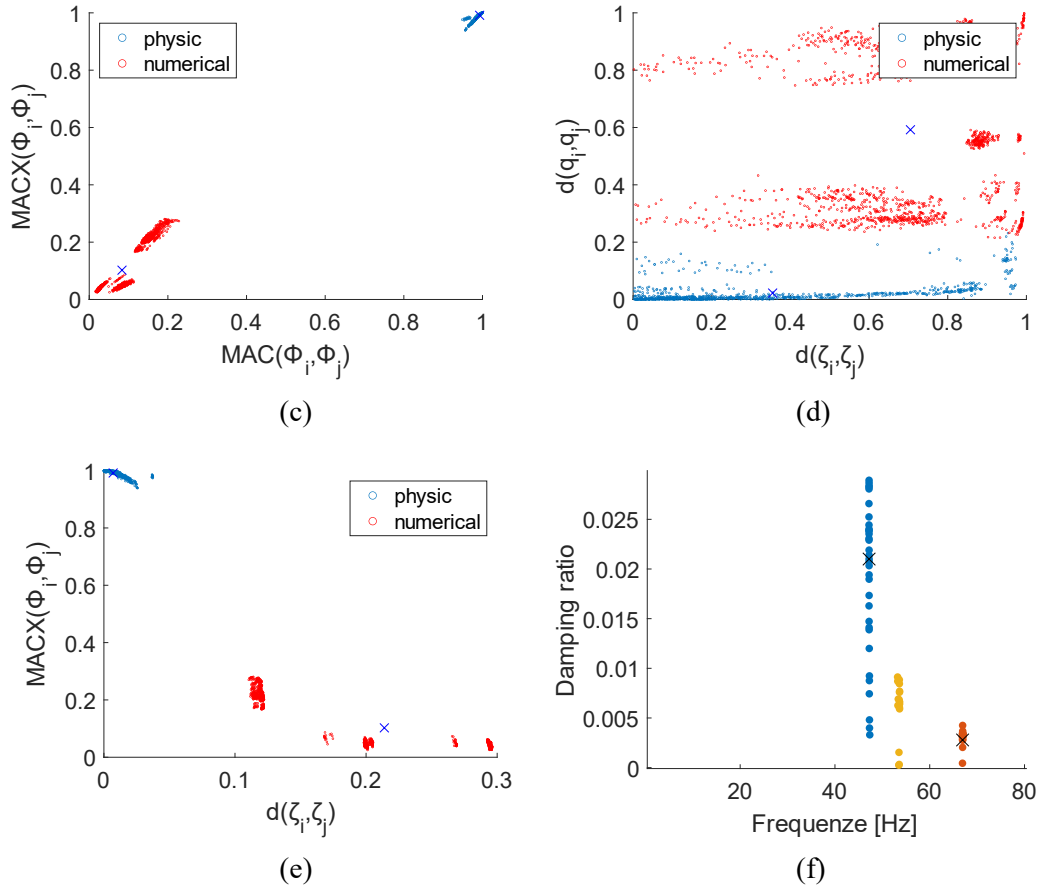


**Fig.3.3.3** The possibly physical modes (blue circle) and certainly spurious modes (red circle), obtained after applying the stabilization (a) eigenvalue distance vs. MAC; (b) frequency distance vs. MAC; (c) MAC vs. MACX; (d) damping ratio distance vs. the modal scaling factors distance; (e) damping ratio distance vs. MACX (the blue cross: final centroids). (f) represent the damping ratio vs. natural frequency diagram of all modes in the physical mode sets (dots), and their representatives (black crosses).

**Table3.15** Through automated selection algorithm, the final natural frequency and damping ratio from Fig.3.3.3 (f)

	Mode 5	Mode 6	Mode 7
Natural frequency (Hz)	47.2	53.6	66.9
Damping ratio (%)	2.1	No value	0.27
Error <sub>NF</sub> (%)	0.26	1.38	0.26
Error <sub>DR</sub> (%)	52.17	No value	86.29

From Table 3.15, it can be seen that the natural frequency is highly similar to the ideal data. But not for the damping ratio, the error is quite large. Obviously, there is no result of the damping ratio in Mode 6.

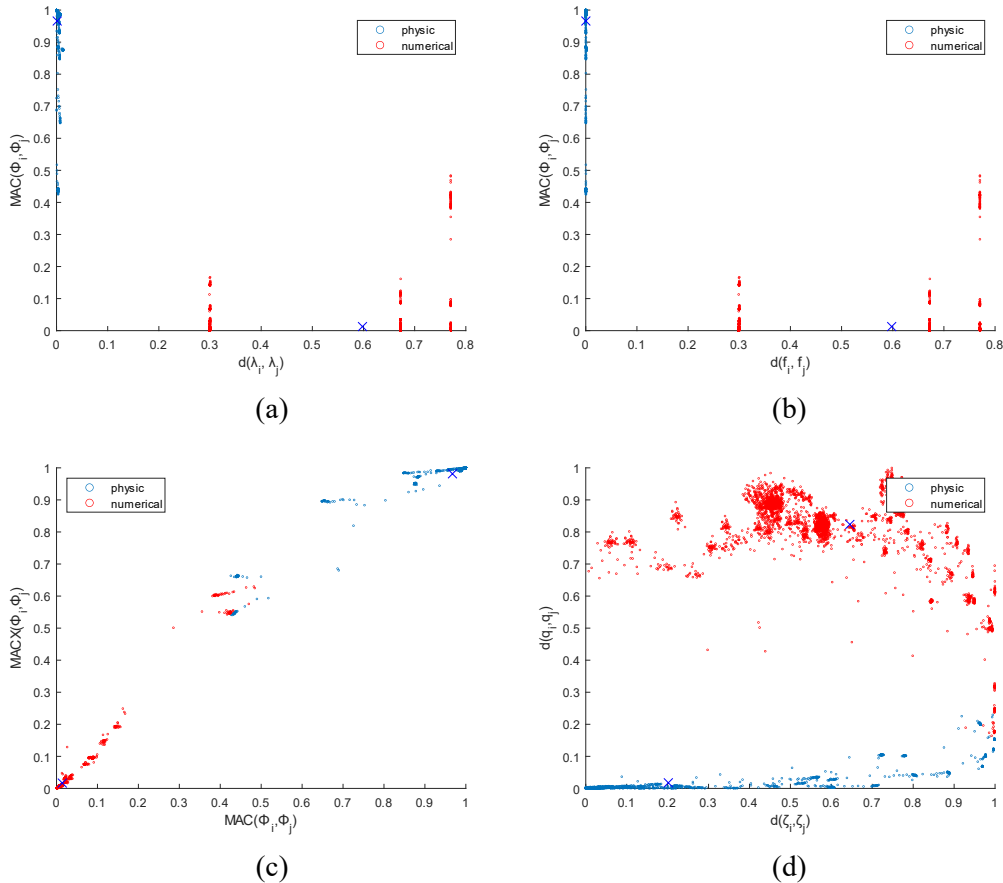
**Table 3.16 The final mode shape through automated selection algorithm**

Mode 5	Mode 6	Mode 7
0.4055 + 2.8301i	-0.2658 + 0.0113i	-0.4799 - 0.0625i
-1.2610 - 0.7721i	-0.1275 + 0.0392i	-0.5921 + 0.1521i
1.0000 + 0.0000i	1.0000 + 0.0000i	1.0000 + 0.0000i
-0.2889 - 0.4314i	-0.1313 + 0.0621i	-0.4981 - 0.1019i
0.5112 - 0.2363i	-0.7132 - 0.2187i	1.2926 - 0.1948i
-0.2566 + 1.0363i	0.1626 + 0.0132i	-0.4028 + 0.2161i
0.0099 - 0.0858i	0.0003 + 0.0043i	-0.0040 - 0.0049i
MAC		
0.6920	0.0303	0.0118

The last row of Table 3.16 is the MAC number of the final mode shape of each mode compare the ideal data. The MAC number of Mode 6 and Mode 7 are highly close to 0. Which means the accuracy of automated selection algorithm for mode shape in this case is bad.

### 3.3.3 CPSD-output only case

Running **ASA.m** in MATLAB by using the data which obtained through **LIPEZ** method CPSD output-only case (case 1:  $N_{\text{FFT}} = 2^{14}$ , mode order = 50, frequency range = 0-100Hz for first three modes; case 2:  $N_{\text{FFT}} = 2^{12}$ , mode order = 50, frequency range = 40-80Hz last four modes). It can be seen that the operation time are 2.45s and 3.05s, and the result can be seen at Fig.3.3.4, Table 3.17, and Table 3.18 for case1 and Fig.3.3.5, Table 3.19, and Table 3.20 for case 2.



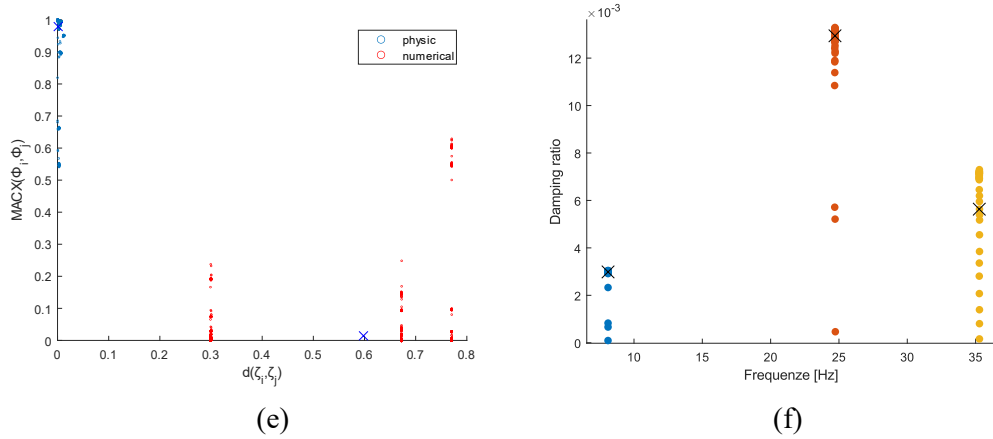


**Fig.3.3.4** The possibly physical modes (blue circle) and certainly spurious modes (red circle), obtained after applying the stabilization (a) eigenvalue distance vs. MAC; (b) frequency distance vs. MAC; (c) MAC vs. MACX; (d) damping ratio distance vs. the modal scaling factors distance; (e) damping ratio distance vs. MACX (the blue cross: final centroids). (f) represent the damping ratio vs. natural frequency diagram of all modes in the physical mode sets (dots), and their representatives (black crosses).

From Fig.3.3.1 and Fig.3.3.2 and Fig.3.3.4, the available data (blue circle) after step 1 are less and less.

**Table3.17** Through automated selection algorithm, the final natural frequency and damping ratio readout from Fig.3.3.4 (f)

	Mode 1	Mode 2	Mode 3
Natural frequency (Hz)	8.1	24.7	35.3
Damping ratio (%)	0.33	1.36	0.62
Error <sub>NF</sub> (%)	0.12	0.00	0.06
Error <sub>DR</sub> (%)	50.00	5.56	56.64

From Table 3.17, the final natural frequency has highly accuracy, but not for the damping ratio, the error is quite large.

**Table 3.18** The final mode shape through automated selection algorithm

Mode 1	Mode 2	Mode 3
0.5136 + 0.0057i	0.7771 + 0.0048i	2.4293 - 0.1271i
0.9880 - 0.0005i	1.2916 + 0.0288i	3.3190 - 0.2992i
1.0000 + 0.0000i	1.0000 + 0.0000i	1.0000 + 0.0000i
1.1647 - 0.0071i	0.7748 - 0.0261i	-2.9200 + 0.0945i
1.1427 + 0.0391i	0.3889 - 0.0453i	-0.2036 + 0.0878i
1.2573 - 0.0022i	-0.3549 - 0.0355i	-3.2326 + 0.2958i
1.3678 - 0.0173i	-2.9095 - 0.0559i	2.3735 - 0.0129i
<b>MAC</b>		
0.9998	0.9995	0.9950

The last row of Table 3.18 is the MAC number of the final mode shape of each mode compare



the ideal data. The MAC number of Mode 1 and Mode 3 are close to 1, which means the accuracy quite high for available mode.

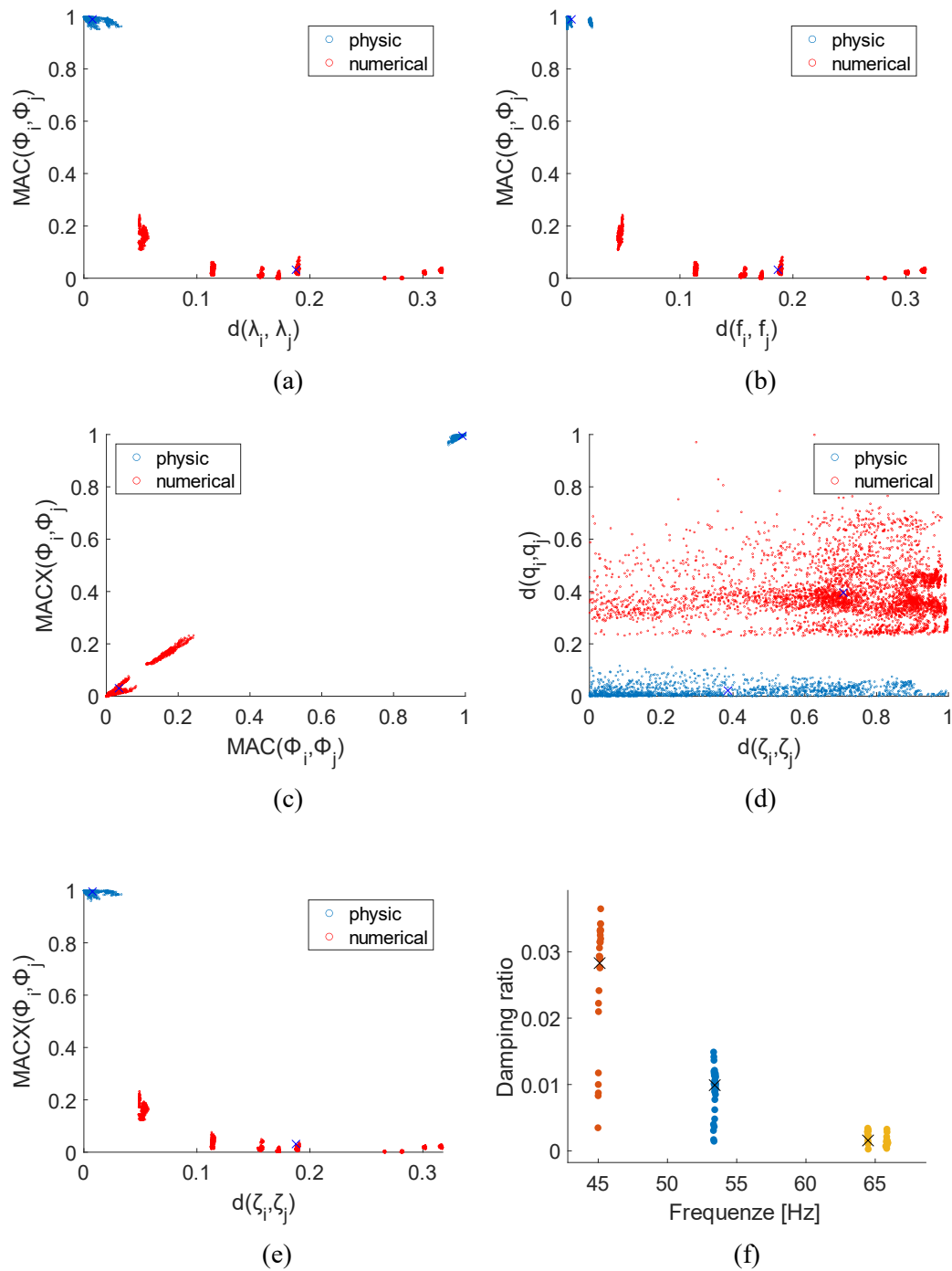


**Fig.3.3.5** The possibly physical modes (blue circle) and certainly spurious modes (red circle), obtained after applying the stabilization (a) eigenvalue distance vs. MAC; (b) frequency distance vs. MAC; (c) MAC vs. MACX; (d) damping ratio distance vs. the modal scaling factors distance; (e) damping ratio distance vs. MACX (the blue cross: final centroids). (f) represent the damping ratio vs. natural frequency diagram of all modes in the physical mode sets (dots), and their representatives (black crosses).

**Table3.19** Through automated selection algorithm, the final natural frequency and

**damping ratio readout from Fig.3.3.5 (f)**

	Mode 4	Mode 5	Mode 6	Mode 7
<b>Natural frequency (Hz)</b>	45	No value	53.4	64
<b>Damping ratio (%)</b>	0.99	No value	0.16	2.83
<b>Error<sub>NF</sub> (%)</b>	0.16	No value	0.11	3
<b>Error<sub>DR</sub> (%)</b>	14	No value	90	46.7

From Table 3.19, the final natural frequency has highly accuracy (expect Mode 5), but not for the damping ratio, the error is quite large.

**Table 3.20 The final mode shape through automated selection algorithm**

Mode 4	Mode 5	Mode 6	Mode 7
-0.5746 -0.0477i	No value	-0.5651 - 2.3831i	-0.2802 + 0.0201i
-0.6456 - 0.0021i	No value	-1.7185 + 0.2423i	-0.1378 + 0.0136i
1.0000 - 0.0000i	No value	1.0000 + 0.0000i	1.0000 + 0.0000i
-0.5195 + 0.0152i	No value	1.7556 + 5.3948i	-0.1434 + 0.0248i
1.5817 - 0.1923i	No value	-1.0515 - 1.4955i	-0.7257 - 0.0068i
-0.5841 + 0.1389i	No value	-1.5437 - 4.6500i	0.1785 - 0.0238i
-0.0895 + 0.0012i	No value	0.4939 + 1.5619i	-0.0071 + 0.0213i
MAC			
0.9177	No value	0.9878	0.9927

The last row of Table 3.20 is the MAC number of the final mode shape of each mode compare the ideal data. There are highly close to 1, which means the accuracy quite high for available mode.

In summary, the accuracy of the automated selection algorithm applied with 3 cases from high to low are input-output, CPSD output-only, and ODS output-only case

Compared with the previous method, using stabilization chart to finding the ‘best’ modal parameter. The automated selection algorithm operation time is shorter, and it does not need to manually increase the limit, and the accuracy is high enough. However, data loss is unavoidable during operation in some cases.

If user want to analyze the changes in the data more clearly, using the first method, which is more intuitive. Although it takes more time and needs to manually set some parameters, it shows that the internal logic of modal parameters estimation and is more friendly to user.

# References

- [1] N. M. M. Maia and J. M. M. Silva, *Theoretical & Experimental Modal Analysis*. John Wiley & Sons, 1997.
- [2] A. Fasana, “Modal parameters estimation in the Z-domain,” *Mech. Syst. Signal Process.*, vol. 23, no. 1, pp. 217–225, 2009.
- [3] E. Reynders, J. Houbrechts, and G. De Roeck, “Fully automated (operational) modal analysis,” *Mech. Syst. Signal Process.*, vol. 29, pp. 228–250, 2012.
- [4] G. Genta, Ed., *Vibration Dynamics and Control*. Boston, MA: Springer US, 2009.
- [5] M. Pastor, M. Binda, and T. Harčarik, “Modal assurance criterion,” *Procedia Eng.*, vol. 48, pp. 543–548, 2012.
- [6] B. P. V. Jacquier, “Extensions of the MAC criterion to complex modes,” in *PROCEEDINGS OF ISMA2010 INCLUDING USD2010*, 2010.
- [7] B. S. &. Richardson, “Measurements Required for Displaying Operating Deflection Shapes,” January 26-29,2004.